

# A comparison between initialization strategies for the infinite hidden Markov model

Federico P. Cortese<sup>\*1,2</sup> and Luca Rossini<sup>†1,3</sup>

<sup>1</sup>Department of Economics, Management, and Quantitative Methods, University of Milan,,  
Via Conservatorio 7, 20122 Milan, Italy

<sup>2</sup>Institute for Applied Mathematics and Information Technologies “E. Magenes” , National  
Research Council, Via Alfonso Corti 12, 20133 Milan, Italy

<sup>3</sup>Fondazione Eni Enrico Mattei, Corso Magenta 63, 20123 Milan, Italy

## Abstract

**Abstract.** Infinite hidden Markov models provide a flexible framework for modelling time series with structural changes and complex dynamics, without requiring the number of latent states to be specified in advance. This flexibility is achieved through the hierarchical Dirichlet process prior, while efficient Bayesian inference is enabled by the beam sampler, which combines dynamic programming with slice sampling to truncate the infinite state space adaptively.

Despite extensive methodological developments, the role of initialization in this framework has received limited attention. This study addresses this gap by systematically evaluating initialization strategies commonly used for finite hidden Markov models and assessing their suitability in the infinite setting.

Results from both simulated and real datasets show that distance-based clustering initializations consistently outperform model-based and uniform alternatives, the latter being the most widely adopted in the existing literature.

**Keywords:** Bayesian nonparametrics; beam sampler; multivariate distributions; regime-switching models; time-series analysis

## 1 Introduction

Regime-switching models offer a flexible framework for modeling multivariate time series characterized by structural changes or dynamic behaviors over time. These models assume the existence of an unobserved latent process that switches between different (usually called  $K$ ) regimes. These shifts among regimes allow to capture nonlinearities, sudden breaks and shifts in dynamics that standard models often fail to represent adequately. Based on their flexibility, regime-switching models have been extensively applied in a wide range of applications, including signal processing [Rabiner, 2002], energy forecasting [Erlwein et al., 2010], biology [Eddy, 1998], and finance [Nystrup et al., 2018].

Within this family, hidden Markov models [HMM, Bartolucci et al., 2013, Zucchini et al., 2017] are particularly effective since they combine latent state dynamics with state-dependent emission distributions that can be specified by the user. However, a long-standing challenge in

---

\*Email: federico.cortese@unimi.it

†Email: luca.rossini@unimi.it

the use of finite HMMs concerns model selection [Buckby et al., 2020], particularly determining the appropriate number of hidden states  $K$ . Since this number is not known a priori, it must be selected through different methods. Common approaches include cross-validation [CV, Stone, 1974], evaluating out-of-sample performance across candidate values, or the use of penalized likelihood (or information) criteria, such as the Akaike’s information criterion [AIC, Akaike, 1974], the Bayesian information criterion [BIC, Schwarz, 1978], and the integrated completed likelihood [ICL, Biernacki et al., 2002]. Although these methods are effective in real data applications, they can be computationally demanding, as they require fitting models over a grid of hyperparameters. Moreover, they can also yield results that depend on sample size, initialization, and choice of the information criteria (see, for example, Bartolucci et al. [2013] and Cortese et al. [2024]).

To overcome these issues, Bayesian nonparametric models have emerged as a natural alternative. These models allow the data to determine the model complexity by assuming an infinite number of latent components, while only a finite subset is effectively used. The foundational idea stems from infinite mixture models [Escobar and West, 1995], which employ a Dirichlet process [DP, Ferguson, 1973] prior over the component distributions. The DP prior allows clustering among data points and it can be extended to hierarchical settings through the hierarchical Dirichlet process [HDP, Teh et al., 2006], which allows multiple mixture models to share a common set of components.

Within the Bayesian nonparametric framework, the infinite hidden Markov model [iHMM, Beal et al., 2001] represents a seminal contribution. This model replaces the transition matrix of the latent Markov process with a HDP prior on it, allowing for a countably infinite set of latent regimes. Its formulation allows the model to automatically infer the number of regimes without the need of an explicit model selection. Moreover, the iHMM can be viewed as a fully Bayesian nonparametric extension of the HMM where both the transition probabilities and the number of regimes are countably infinite and are inferred directly from the data, which determines the model complexity.

Since its introduction, iHMM has been widely extended and applied to different applications. For instance, Song [2014] specifies an iHMM with Gaussian autoregressive (AR) regimes for U.S. real interest rates, while Shi and Song [2015] use an iHMM to detect speculative bubbles in U.S. housing ratios. Maheu and Yang [2016] incorporate the iHMM within continuous time Vasicek [1977] model for U.S. short-term interest rates and Hou [2017] applies a vector autoregressive (VAR) iHMM to macroeconomic forecasting. Yang [2019] extends the iHMM to capture relationships between stock returns and economic growth, while Jin and Maheu [2016] introduce an iHMM with Wishart observations for low-dimensional realized covariance matrices, and Jin et al. [2019] extend it to high-dimensional realized covariance matrices via dynamic factor models, applied to large S&P 500 panels. Beyond financial econometrics, Hoskovec et al. [2023] develop an iHMM for asynchronous multivariate series with missing data using a covariate-dependent probit stick-breaking process, applied to air pollution exposure.

Despite the growing interest in iHMMs, an important aspect concerns the role of initialization in posterior inference. Estimation of the iHMM typically relies on the beam sampler [Van Gael et al., 2008], a blocked Gibbs sampling algorithm that efficiently handles the infinite latent state space. Although Van Gael et al. [2008] argue that the beam sampler is robust to initialization and recommend using a uniform initialization for the latent states, no systematic analysis has yet examined how different initialization strategies affect its behavior. In contrast, the literature on finite HMMs and mixture models shows that inference results, particularly when relying on the expectation–maximization (EM) algorithm [Dempster et al., 1977], can strongly depend on the initialization of latent states [Pandolfi et al., 2023]. For finite HMM, Maruotti and Punzo [2021] perform an extensive comparison of several initialization strategies, such as  $k$ -means, partitioning around medoids [Kaufman and Rousseeuw, 1987, 2009], hereafter referred to as *pam*, and *Gaussian mixtures* [McLachlan and Peel, 2000]. Their results indicate that  $k$ -means often performs best overall, Gaussian mixtures are more effective in high-dimensional settings, and *pam* offers advantages in low-dimensional cases. However, these results are limited to finite-state HMM and to data generated from a multivariate Gaussian distribution, leaving open the

question of how initialization affects inference in nonparametric, infinite-state models.

Our main purpose is to examine how different initialization strategies influence the performance of the beam sampler in the multivariate Gaussian iHMM. To the best of our knowledge, this is the first study to systematically investigate initialization strategies within the iHMM framework. Indeed, we aim to bridge the gap between finite HMMs and iHMMs by evaluating how initialization methods commonly employed in the former model perform when applied to the latter. Specifically, we consider four standard approaches used in classical HMM estimation: uniform initialization as proposed by Van Gael et al. [2008],  $k$ -means and pam based on the GAP statistic [Witten and Tibshirani, 2010], and Gaussian mixture models [McLachlan and Peel, 2000] guided by information criteria such as the BIC.

To test these methods, we perform two extensive simulation studies: one considering Gaussian data and one with Student- $t$  data with fat tails, to assess performance under both standard and heavy-tailed conditions, the latter being a setting that better reflects real-world scenarios. This is done to investigate the performance of each initialization strategy under a misspecified model formulation, and consequently to assess the robustness of both the beam sampler and the initialization strategies. We evaluate the performance of the strategies by testing (i) their ability to recover the true latent structure, measured by the adjusted Rand index (ARI; Hubert and Arabie, 1985) at convergence, and (ii) their convergence speed, measured by changes in ARI across iterations. As a further measure, we evaluate the ability of the beam sampler and the initialization strategies to converge through the Geweke [1992] diagnostic and the autocorrelation time (ACT).

Once we assess the performance of the initialization methods in simulation, we apply the iHMM to two real datasets: (1) the monthly industrial production volume index for nine European countries from March 2002 to August 2025, and (2) the *Old Faithful* geyser dataset, a well-known benchmark in time series clustering analysis.

Results indicate that  $k$ -means and pam generally outperform Gaussian mixtures initializations, particularly when the data-generating process violates the Gaussianity assumption or when different clusters exhibit substantial overlap. In contrast, the uniform initialization performs poorly in nearly all scenarios, suggesting that it should be avoided in practice. The choice of initialization also affects model performance on real data. For the Old Faithful geyser dataset, results are largely consistent across initialization schemes, whereas for the industrial production volume dataset, which is an inherently more complex scenario, initialization has a substantial impact on the final model estimates, with  $k$ -means and pam yielding consistent and more robust classification.

The paper is organized as follows. Section 2 presents the formulation of the multivariate Gaussian iHMM and the beam sampler. Section 3 discusses the initialization strategies considered, while Section 4 shows two extensive simulation studies assessing their accuracy and convergence under different scenarios. Section 5 presents two empirical studies where we model real-world time series with an iHMM. Section 6 concludes.

## 2 Methodology

Selecting the appropriate number of components in mixture and regime-switching models is a well-known challenge. Classical approaches typically rely on likelihood-based model selection criteria or cross-validation, which are often sensitive to the number of regimes specified a priori. Bayesian nonparametric methods offer an elegant alternative by allowing the model complexity to adapt flexibly to the data. Rather than fixing the number of latent states in advance, these models infer it directly from the data through prior constructions that support a potentially infinite number of components [Ghosh and Ramamoorthi, 2003, Hjort et al., 2010, Müller et al., 2015].

This approach is based on the Dirichlet process [DP, Ferguson, 1973], which defines a prior over distributions and induces mixture models with a countably infinite number of components. Several extensions of the DP mixtures have been proposed, demonstrating its versatility in

classification and density estimation [Fuentes-García et al., 2010, Gutiérrez et al., 2014]. The HDP introduced by Teh et al. [2006] generalizes this framework by allowing multiple groups to share a common set of mixture components. This hierarchical construction provides the foundation for iHMM.

## 2.1 The infinite hidden Markov model

We begin by briefly revisiting the finite HMM before introducing its infinite, nonparametric extension. Consider a multivariate continuous time series  $\mathbf{y}_1, \dots, \mathbf{y}_T$ , where  $\mathbf{y}_t \in \mathbb{R}^P$ , and assume the existence of a latent first-order Markov process  $\mathbf{s}$  with components

$$s_1, \dots, s_T, \quad s_t \in \mathbb{N},$$

where each  $s_t$  takes values in  $\{1, 2, \dots, K\}$ . The model for  $s_1, \dots, s_T$  specifies transition probabilities  $\pi_{ij}(t) = \mathbb{P}(s_t = j | s_{t-1} = i)$ , and initial state probabilities  $\pi_i = \mathbb{P}(s_1 = i)$ , for  $i, j \in \{1, \dots, K\}$ . Conditional on the latent state  $s_t$ , the observation  $\mathbf{y}_t$  is generated from a state-specific emission distribution  $f(\cdot | \boldsymbol{\theta}_{s_t})$ . Assuming conditional independence of the  $\mathbf{y}_t$  given the states  $s_t$ , the joint distribution of states and observations is

$$f(s_1, \dots, s_T, \mathbf{y}_1, \dots, \mathbf{y}_T) = \pi_{s_1} f(\mathbf{y}_1 | \boldsymbol{\theta}_{s_1}) \prod_{t=2}^T \pi_{s_{t-1}, s_t}(t) f(\mathbf{y}_t | \boldsymbol{\theta}_{s_t}).$$

While the classical HMM assumes a finite number of states  $K$ , this can be restrictive in practice. The infinite HMM relaxes this constraint by allowing the number of regimes to be potentially unbounded, which is achieved by assigning each row of the transition matrix an infinite-dimensional probability vector

$$\boldsymbol{\pi}_k = (\pi_{k1}, \pi_{k2}, \dots), \quad k = 1, 2, \dots$$

We place a hierarchical DP prior on each row

$$\boldsymbol{\pi}_k | G_0, \alpha \sim \text{DP}(\alpha, G_0), \quad G_0 | \gamma \sim \text{DP}(\gamma, H),$$

where  $H$  is the base measure and  $\alpha$  and  $\gamma$  are concentration parameters. This hierarchical structure induces that state-specific transition distributions  $\boldsymbol{\pi}_k$  share a common set of states, which supports a countably infinite number of regimes [Teh et al., 2006].

Using the stick-breaking representation [Sethuraman, 1994], we write  $G_0 = \sum_{k'=1}^{\infty} \beta_{k'} \delta_{\boldsymbol{\theta}_{k'}}$  and  $G_k = \sum_{k'=1}^{\infty} \pi_{kk'} \delta_{\boldsymbol{\theta}_{k'}}$ , where  $\boldsymbol{\beta} = (\beta_1, \beta_2, \dots)' \sim \text{GEM}(\gamma)$  are the global stick-breaking weights representing the mixture proportions shared across all states, and  $\boldsymbol{\theta}_k \sim H$ . Identifying each  $G_k$  with both transition probabilities  $\pi_{kk'}$  and emission parameters  $\boldsymbol{\theta}_k$  allows us to formally define the iHMM as

$$\begin{aligned} \boldsymbol{\pi}_k &\sim \text{DP}(\alpha, \boldsymbol{\beta}), \\ \boldsymbol{\beta} &\sim \text{GEM}(\gamma), \\ \boldsymbol{\theta}_k &\sim H, \\ s_t | s_{t-1} &\sim \text{Multinomial}(\boldsymbol{\pi}_{s_{t-1}}), \\ \mathbf{y}_t | s_t &\sim f(\cdot | \boldsymbol{\theta}_{s_t}). \end{aligned} \tag{1}$$

In this paper, we focus on the multivariate Gaussian iHMM, where conditional on the regime indicator  $s_t$ , the observations follow

$$\mathbf{y}_t | s_t = k, \boldsymbol{\mu}_k, \boldsymbol{\Sigma}_k \sim \mathcal{N}_P(\boldsymbol{\mu}_k, \boldsymbol{\Sigma}_k),$$

and each pair  $(\boldsymbol{\mu}_k, \boldsymbol{\Sigma}_k)$  is assigned a Normal-Inverse-Wishart (NIW) prior

$$\boldsymbol{\Sigma}_k \sim \mathcal{IW}(\nu_0, \boldsymbol{\Lambda}_0), \quad \boldsymbol{\mu}_k | \boldsymbol{\Sigma}_k \sim \mathcal{N}_P(\boldsymbol{\mu}_0, \boldsymbol{\Sigma}_k / \kappa_0),$$

where  $\nu_0$  and  $\mathbf{\Lambda}_0$  are the degrees of freedom and the scale matrix, respectively. Regarding the choice of the hyperparameters, we adopt vague priors with  $\boldsymbol{\mu}_0 = \mathbf{0}$ ,  $\mathbf{\Lambda}_0 = \mathbf{I}_P$ ,  $\kappa_0 = 0.01$ , and  $\nu_0 = P + 2$ .

To complete the model specification, we place Gamma hyperpriors on the concentration parameters controlling regime persistence ( $\alpha$ ) and complexity of the model ( $\gamma$ )

$$\begin{aligned}\alpha &\sim \text{Gamma}(a_\alpha, b_\alpha), \\ \gamma &\sim \text{Gamma}(a_\gamma, b_\gamma).\end{aligned}$$

Following [Van Gael et al. \[2008\]](#), in the simulation studies of Section 4 and in the empirical analysis of Section 5, we place vague priors by setting  $a_\alpha = 1$ ,  $b_\alpha = 1$ ,  $a_\gamma = 2$ , and  $b_\gamma = 1$ . This specification minimizes the impact on the estimation of the number of states, allowing us to better observe the behavior of each initialization strategy under comparable conditions.

A graphical representation of the iHMM structure is provided in Figure 1, where the hierarchy between  $\boldsymbol{\beta}$ ,  $\boldsymbol{\pi}_k$  and  $\boldsymbol{\theta}_k$  captures the sharing of regimes across transition rows while allowing an unbounded number of latent states.

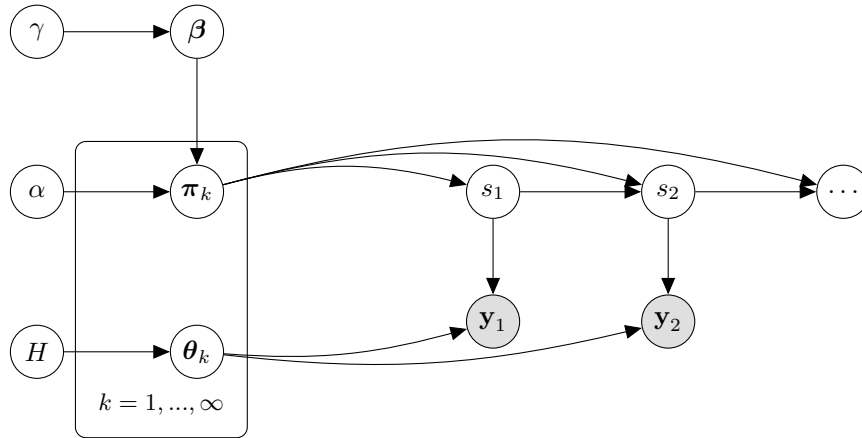


Figure 1: Direct Acyclic Graph (DAG) of the infinite hidden Markov model. It exhibits the hierarchical structure of priors, where directed arrows show the causal dependence structure of the model.

## 2.2 Posterior inference

[Beal et al. \[2001\]](#) first introduce the iHMM and present a fully Bayesian framework that extends conventional HMMs to a countably infinite number of latent states. Their approach relies on DP priors to model the transition and emission distributions, and inference is carried out using an approximate Gibbs sampling scheme that alternates updating the latent state sequence and the model hyperparameters.

Building on this work, [Teh et al. \[2006\]](#) define the HDP as a general Bayesian nonparametric prior for grouped data, showing that the iHMM arises as a special case of this hierarchical construction. This HDP allows each group-specific DP to share atoms through a global base measure drawn from another DP. They also derive an efficient Gibbs sampling algorithm based on the Chinese restaurant franchise and stick-breaking representation. However, because time series data typically exhibit strong temporal dependencies between consecutive time steps, Gibbs sampling often converges slowly [[Scott, 2002](#)]. To mitigate this, [Fox et al. \[2011\]](#) propose an alternative sampling method called the sticky HDP-HMM, which introduces an additional hyperparameter to control self-transition probabilities, while reducing label-switching.

In this study, we employ the beam sampler introduced by Van Gael et al. [2008], due to its computational efficiency and improved convergence properties. The method combines the *slice sampling* [Walker, 2007, Kalli et al., 2011] with dynamic programming, providing an efficient alternative to Gibbs sampling. The key idea is to introduce auxiliary *slice variables*  $\mathbf{u} = (u_1, \dots, u_T)$  that, at each iteration, restrict the number of feasible state trajectories to a finite subset of the infinite state space. Conditioned on these variables, only transitions satisfying  $\pi_{s_{t-1}, s_t} > u_t$  remain feasible, thus enabling the use of the forward-filtering backward-sampling (FFBS) algorithm [Dempster et al., 1977, Chib, 1996], a standard tool in finite HMM inference [Zucchini et al., 2017]. Subsequently, the transition probabilities  $\boldsymbol{\pi}_k$  are drawn from  $\text{DP}(\alpha, \boldsymbol{\beta})$ , with each row of the transition matrix updated according to the current transition counts, while the global stick-breaking weights  $\boldsymbol{\beta}$  are sampled from a Dirichlet posterior using auxiliary table counts, as described in Teh et al. [2006]. Emission parameters  $\boldsymbol{\theta}_k$  are then resampled given the observations assigned to each state; in the Gaussian case, each pair  $\boldsymbol{\theta}_k = (\boldsymbol{\mu}_k, \boldsymbol{\Sigma}_k)$  is updated from a NIW posterior. Finally, the hyperparameters  $\alpha$  and  $\gamma$  are drawn from Gamma posteriors.

The computational complexity per iteration is  $O(TK^2)$  in the worst case, but typically much lower since most transitions are excluded by the slice variables [Van Gael et al., 2008]. A schematic implementation of the beam sampler is provided in Algorithm 1.

---

**Algorithm 1** Beam sampler for the iHMM

---

- 1: Initialize  $\mathbf{s}, \boldsymbol{\pi}_k, \boldsymbol{\beta}, \{\boldsymbol{\theta}_k\}, \alpha, \gamma$
  - 2: **for** iteration  $i = 1, \dots, N$  **do**
  - 3:     **for**  $t = 1, \dots, T$  **do**
  - 4:         Sample  $u_t \sim \text{Uniform}(0, \pi_{s_{t-1}, s_t})$
  - 5:     **end for**
  - 6:     Sample  $\mathbf{s}$  via FFBS restricted to  $\pi_{s_{t-1}, s_t} > u_t$
  - 7:     Sample  $\boldsymbol{\pi}_k \mid \mathbf{s}, \boldsymbol{\beta}, \alpha \sim \text{DP}(\alpha, \boldsymbol{\beta})$
  - 8:     Sample  $\boldsymbol{\beta} \mid \mathbf{s}, \gamma$  using auxiliary table counts
  - 9:     Sample emission parameters  $\boldsymbol{\theta}_k \mid \mathbf{s}, \mathbf{y}_1, \dots, \mathbf{y}_T$  (e.g. NIW posterior)
  - 10:     Sample hyperparameters  $\alpha, \gamma$  from Gamma posteriors
  - 11: **end for**
- 

### 3 Initialization strategies

Our main objective is to investigate how different initialization strategies affect the performance of the beam sampler when estimating the multivariate Gaussian iHMM. While initialization has been studied extensively in the context of finite HMM literature [see, e.g., Maruotti and Punzo, 2021, Pandolfi et al., 2023], to our knowledge, our paper is the first work that systematically analyzes initialization procedures in the iHMM framework. Because the iHMM generalizes the finite HMM by allowing an unbounded number of regimes, it is not obvious whether initialization methods that work well for finite models will remain effective when the state space is theoretically infinite.

To bridge the gap between finite and infinite hidden Markov models, we evaluate four initialization strategies that are widely used in HMM estimation and clustering analysis. These strategies – uniform initialization,  $k$ -means clustering, partitioning around medoids (pam), and Gaussian mixture modeling – represent complementary approaches that differ in their underlying assumptions and computational mechanisms. By systematically comparing their performance within the iHMM framework, we aim to clarify how initialization choices influence convergence behavior and posterior inference.

- (i) **Uniform initialization.** The latent states are assigned randomly as

$$s_t \sim \mathcal{U}\{1, \dots, K_0\}, \quad K_0 \sim \mathcal{U}\{2, 3, 4, 5\},$$

where  $\mathcal{U}\{\dots\}$  is a discrete uniform distribution. This procedure, originally proposed by [Van Gael et al. \[2008\]](#), provides a baseline where no prior information is imposed. Since the latent allocations are drawn uniformly, it allows the beam sampler to explore the state space broadly initially.

- (ii) ***k*-means clustering.** It partitions the data into  $K$  clusters by minimizing the within-cluster sum of squares

$$\min_{\{\boldsymbol{\mu}_k\}_{k=1}^K} \sum_{t=1}^T \|\mathbf{y}_t - \boldsymbol{\mu}_{s_t}\|^2, \quad s_t \in \{1, \dots, K\},$$

where  $\{\boldsymbol{\mu}_k\}_{k=1}^K$  are the centroids. The optimal number of clusters  $K$  is determined by using the GAP statistic [[Witten and Tibshirani, 2010](#)], which compares the observed within-cluster dispersion to that expected under a null reference distribution

$$\text{GAP}(K) = \mathbb{E}[\log(W_K^*)] - \log(W_K),$$

where  $W_K$  denotes the within-cluster sum of squares for a given partition into  $K$  clusters, and  $W_K^*$  is the same measure computed from permuted data. A larger GAP value indicates stronger cluster separation relative to random noise.

We use 25 permutations and compute the statistic through the *clusGap* function from the **cluster** package [[Maechler et al., 2025](#)] in R [[R Core Team, 2021](#)]. However, since many selection rules can be applied when using the GAP statistic, we adopt the global maximum criterion, which selects the number of clusters  $K$  corresponding to the highest GAP value across all candidates. This approach is the least conservative<sup>1</sup>, favoring broader exploration of the parameter space.

- (iii) **pam algorithm** [[Kaufman and Rousseeuw, 1987, 2009](#)]. It is conceptually similar to *k*-means but minimizes distances from representative *medoids* instead of centroids. This makes pam more robust to outliers and to non-spherical cluster shapes. As for *k*-means, the number of clusters is selected through the GAP statistic with 25 permutations. The model is fitted using the *pam* function from the **cluster** R package.
- (iv) **Gaussian mixtures initialization**, or referred to simply as *mixtures*. In this approach, each observation is modeled as arising from a mixture of  $K$  multivariate Gaussian components

$$f(\mathbf{y}_t) = \sum_{k=1}^K \phi_k \mathcal{N}_p(\mathbf{y}_t \mid \boldsymbol{\mu}_k, \boldsymbol{\Sigma}_k),$$

where  $\phi_k$  are mixture weights satisfying  $\sum_k \phi_k = 1$ .

The number of components  $K$  is selected according to the Bayesian Information Criterion [BIC, [Schwarz, 1978](#)], defined as

$$\text{BIC} = -2 \ell(\hat{\boldsymbol{\theta}}) + q \log(T),$$

where  $\ell(\hat{\boldsymbol{\theta}})$  is the maximized log-likelihood,  $q$  is the number of free parameters, and  $T$  the sample size. Lower BIC values indicate a better trade-off between model fit and complexity. We fit the model using the *Mclust* function from the **mclust** R package [[Fraley et al., 2012](#)], which automatically fits candidate models and selects the optimal  $K$  by BIC comparison.

---

<sup>1</sup>In the simulation settings, when using *k*-means or pam as initialization strategies, we also applied the [Witten and Tibshirani \[2010\]](#) rule for model selection, which selects the cluster size  $k$  as the smallest value satisfying  $\text{GAP}(k) \geq \text{GAP}(k+1) - s_{k+1}$ , where  $s_{k+1}$  is the standard deviation estimated from the bootstrap samples used to compute  $\text{GAP}(k+1)$ . That said, its tendency to be overly conservative often limited exploration of the state space.

Since GAP statistic and BIC require a maximum number of clusters, we evaluate candidate values of  $K$  ranging from 2 to 5, and select the optimal starting point accordingly. It is worth noting that this maximum number also constrains the parameter search space; however, our choice is justified by both computational reasons and empirical relevance. From a computational perspective, the GAP statistic requires re-estimating the clustering solution (in our case, via  $k$ -means or pam)  $n$  times, where  $n$  is the number of bootstrap samples. This significantly increases computational time, especially in high-dimensional or long time series settings. From an empirical viewpoint, many real-world applications, such as financial time series segmentation, natural language processing, or gene expression analysis [Nystrup et al., 2021], require a limited number of states for both interpretability and ease of estimation. Moreover, considering that we place vague hyperpriors on the concentration parameters  $\alpha$  and  $\gamma$  of the DPs described in Eq. (1), this constraint does not materially affect the results, as the model remains flexible enough to recover all relevant states.

## 4 Simulation study

To evaluate the impact of the different initialization strategies on the performance of the beam sampler in the multivariate Gaussian iHMM, we rely on two different simulation experiments. The first investigates the performance under model correctness, where the data-generating process follows a multivariate Gaussian HMM. The second examines the robustness to model misspecification, using data generated from a multivariate Student- $t$  HMM with heavy tails, specifically with  $\nu = 5$  degrees of freedom. These two experiments allow us to assess the robustness of both the model and the initialization procedures.

We generate synthetic datasets from a finite-state HMM with  $K$  latent states. Each regime is characterized by its own-state specific mean or location vector  $\boldsymbol{\mu}_k$  and covariance matrix  $\boldsymbol{\Sigma}_k$ , and the corresponding transition matrix is constructed to control regime persistence. Specifically, we fix the diagonal elements of the transition matrix equal to

$$\pi_{ii} = 0.95, \quad i = 1, \dots, K,$$

so that each regime is highly persistent, while the off-diagonal elements satisfy

$$\pi_{ij} = \frac{1 - \pi_{ii}}{K - 1} = \frac{0.05}{K - 1}, \quad i \neq j.$$

This specification ensures a realistic level of regime persistence without inducing degenerate transitions. Emission distributions are drawn from a multivariate Gaussian distribution (for the correctly specified scenario, see Section 4.1) or from a multivariate Student- $t$  distribution with  $\nu = 5$  degrees of freedom (for the misspecified scenario, see Section 4.2), which represent an heavy-tailed behavior as often observed in the economic or financial applications.

To explore a wide range of data-generating conditions, we vary

$$\omega \in \{0, 0.10\}, \quad K \in \{2, 4\}, \quad T \in \{500, 1000\}, \quad P \in \{5, 20\},$$

where  $K$  represent the number of states,  $P$  the number of variables and  $T$  the time dimensionality of the dataset. Moreover,  $\omega$  is the overlap measure, which quantifies the degree of separation between clusters or regimes. This parameter is defined following Maitra and Melnykov [2010] and controls the expected probability of overlap between two distinct clusters. To generate realistic cluster configurations, we rely on the **MixSim** R package [Melnykov et al., 2012], which provides direct control over  $\omega$ . Figure 2 provides an illustration of how  $\omega$  influences cluster uncertainty, highlighting that a smaller  $\omega$  yields well-separated clusters (left panel), whereas a larger value indicates greater overlap (right panel).

For each combination of  $\omega$ ,  $K$ ,  $T$  and  $P$ , we generate 50 independent replications, resulting in a total of 3200 datasets. Each dataset is then fitted with an iHMM using the four initialization strategies described in Section 3 (uniform,  $k$ -means, pam, and mixtures). Unless otherwise

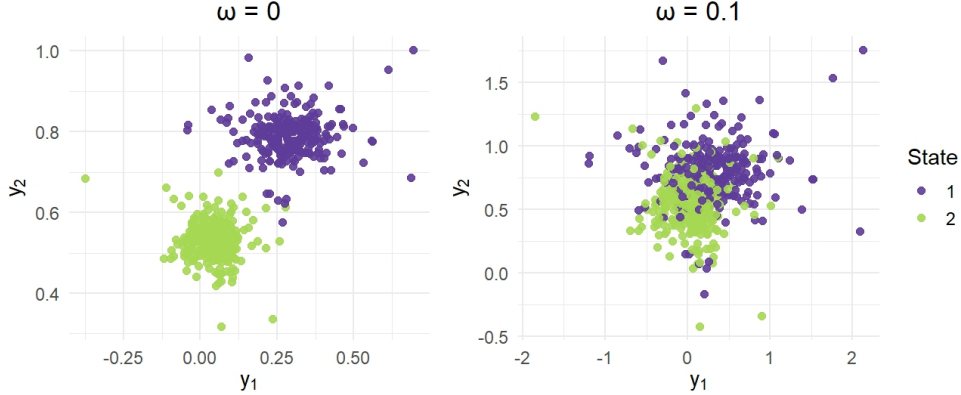


Figure 2: Effect of the overlap parameter  $\omega$  on the separation between clusters for data simulated from a Student- $t$  distribution with  $\nu = 5$ ,  $K = 2$ ,  $T = 500$ , and  $P = 2$ .

stated, we employ 1500 iterations of the beam sampler without burn-in or thinning to assess the convergence speed.

We evaluate the classification accuracy and the convergence speed of each initialization method by employing the Adjusted Rand Index [ARI, Hubert and Arabie, 1985] computed between true and estimated sequences of latent states, and across all random seeds and iterations. ARI measures the extent to which two partitions overlap: let us denote with  $C^{(m)} = \{C_1^{(m)}, \dots, C_h^{(m)}\}$  the partition obtained with a generic clustering algorithm, which yields  $h$  clusters on a set of  $n$  elements, and with  $C^{(r)} = \{C_1^{(r)}, \dots, C_d^{(r)}\}$  the real clustering, consisting of  $d$  groups. Consider the following contingency table

	$C_1^{(m)}$	$C_2^{(m)}$	$\dots$	$C_h^{(m)}$	$\sum_{j=1}^h n_{ij}$
$C_1^{(r)}$	$n_{11}$	$n_{12}$	$\dots$	$n_{1h}$	$a_1$
$C_2^{(r)}$	$n_{21}$	$n_{22}$	$\dots$	$n_{2h}$	$a_2$
$\vdots$	$\vdots$	$\vdots$	$\ddots$	$\vdots$	$\vdots$
$C_d^{(r)}$	$n_{d1}$	$n_{d2}$	$\dots$	$n_{dh}$	$a_d$
$\sum_{i=1}^d n_{ij}$	$b_1$	$b_2$	$\dots$	$b_h$	$n$

where  $n_{ij}$  is the count of elements common to clusters  $C_i^{(m)}$  and  $C_j^{(r)}$ ,  $a_i = \sum_j n_{ij}$ , and  $b_j = \sum_i n_{ij}$ . Then,  $\text{ARI}(C^{(r)}, C^{(m)})$  is calculated as [Das and Biswas, 2023]

$$\text{ARI}(C^{(r)}, C^{(m)}) := \frac{\sum_j \sum_i \binom{n_{ij}}{2} - \frac{[\sum_i \binom{a_i}{2}] \sum_j \binom{b_j}{2}}{\binom{n}{2}}}{\frac{1}{2} \left[ \sum_i \binom{a_i}{2} + \sum_j \binom{b_j}{2} \right] - \frac{[\sum_i \binom{a_i}{2}] \sum_j \binom{b_j}{2}}{\binom{n}{2}}}.$$

It essentially checks, for every pair of observations, whether the two clusterings place a specific pair together or apart, and then compares the overall level of agreement. Because some agreement would occur just by chance, the ARI subtracts this expected random agreement. To compute ARI, we use the R function *adjustedRandIndex* from the **mclust** package.

In our simulation study, we summarize the ARI across seeds and iterations for each configuration of the simulation parameters, and report its summary statistics at convergence of the beam sampler. Additionally, in Section 4.3, we examine the convergence of the beam sampler

under each initialization method using the Geweke [1992] convergence diagnostic and the auto-correlation time (ACT), which assess the similarity of early and late samples and the level of serial dependence in the Markov Chain Monte Carlo (MCMC) draws.

#### 4.1 First scenario: Gaussian data

The first scenario examines the performance of the four initialization strategies when the data are generated from a HMM with Gaussian emission distributions. This setting corresponds to a correctly specified model and allows us to evaluate convergence dynamics and classification accuracy under ideal conditions.

Figure 3 reports the evolution of the median ARI across 1 500 iterations (top panel) and the distribution of ARI values at convergence (bottom panel)<sup>2</sup>. All initialization strategies show improvements in ARI over iterations but their rates of convergence differ substantially. The  $k$ -means, pam, and Gaussian mixtures initializations achieve rapid increases in ARI during the first iterations, reaching perfect (ARI around 1) classification in most replications. However, the uniform initialization converges slowly and shows greater variability across simulation replications, reflecting the instability of purely random starting partitions.

Table 1 compares results for  $\omega = 0$  and  $\omega = 0.10$ , corresponding to clearly and weakly separated clusters, respectively. In low-overlap conditions ( $\omega = 0$ ), all methods recover the correct latent sequence, yielding ARI values close to 1, with  $k$ -means and pam approaches displaying lower variance across replications. However, as overlap increases ( $\omega = 0.1$ ), performance differences become more pronounced. The  $k$ -means initialization remains the most robust to reduced separation, with median ARI values exceeding 0.9 and exhibiting narrower confidence intervals and lower ARI variability. The mixture-based and the pam initializations deteriorate moderately, while uniform initialization often underestimates the number of correct states and exhibits wide dispersion in ARI values.

We analyse also the impact of the true number of regimes ( $K$ ) by focusing on two and four states. When  $K = 2$ , all initialization methods exhibit accurate recovery of the true number of states, but uniform initialization tends to over-estimate the number of states creating extra regimes. When  $K = 4$ , the complexity of the latent structure increases, and the uniform and mixture initializations show higher dispersion in the estimated number of regimes, whereas  $k$ -means and pam continue to recover the correct  $K$  with high consistency. This suggests that more structured and non-parametric initialization methods might help the sampler to avoid local posterior modes associated with redundant states.

Table 1: Median, 2.5% and 97.5% quantiles and standard deviation (SD) of ARI, and estimated number of states  $\hat{K}$ , across initialization methods, for different  $\omega$  and  $K$ , with data simulated from a Gaussian distribution. Highest ARI median and lowest ARI standard deviation are highlighted in bold.

Method	Median	2.5%	97.5%	SD	Median	2.5%	97.5%	SD	$\hat{K}$
	$\omega = 0$				$K = 2$				
$k$ -means	<b>1.00</b>	0.97	1.00	0.01	0.98	0.90	1.00	0.06	<b>2.0</b>
mixtures	<b>1.00</b>	0.66	1.00	0.09	<b>1.00</b>	0.90	1.00	<b>0.04</b>	<b>2.0</b>
pam	<b>1.00</b>	1.00	1.00	<b>0.00</b>	0.98	0.87	1.00	0.13	<b>2.0</b>
uniform	0.98	0.48	1.00	0.21	0.96	0.00	1.00	0.25	3.0
	$\omega = 0.10$				$K = 4$				
$k$ -means	<b>0.92</b>	0.33	0.98	<b>0.23</b>	<b>0.98</b>	0.34	1.00	<b>0.24</b>	<b>4.0</b>
mixtures	0.91	0.00	0.98	0.26	0.85	0.00	1.00	0.27	3.0
pam	0.91	0.00	0.98	0.29	<b>0.98</b>	0.00	1.00	0.29	<b>4.0</b>
uniform	0.88	0.00	0.98	0.33	0.69	0.00	1.00	0.28	3.5

<sup>2</sup>We provide additional results in the supplementary material.

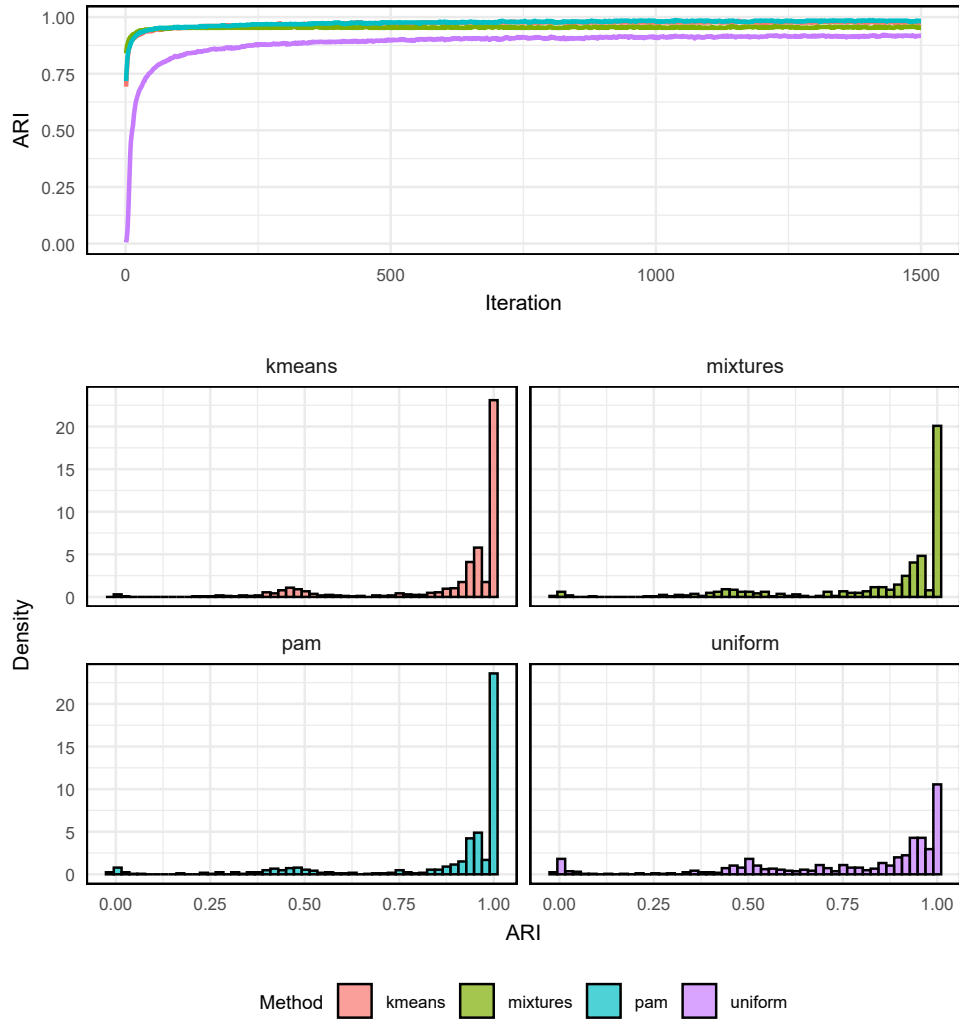


Figure 3: Median ARI across 50 seeds at each iteration computed between true and estimated latent sequences (top panel) and histograms of ARI values at convergence (bottom) for all initialization methods. Results refer to data simulated from a Gaussian distribution.

Figure 4 displays the median ARI across iterations by focusing on the sequence length  $T$  (top panel) and the number of variables  $P$  (bottom panel). When  $T$  increases from 500 to 1000 observations, all initialization schemes benefit from the additional information, achieving smoother ARI trajectories and reducing variability. We notice that uniform initialization always outperforms the other methods in negative, while the remaining methods seem to reach convergence in the first iterations.

The results are different when looking at the number of variables  $P$ . When it increases from 5 to 20, both  $k$ -means and pam maintain high accuracy, whereas mixture initialization decreases, due to the difficulty of estimating full covariance matrices in high-dimensional spaces. Uniform initialization deteriorates with the dimensionality, as expected.

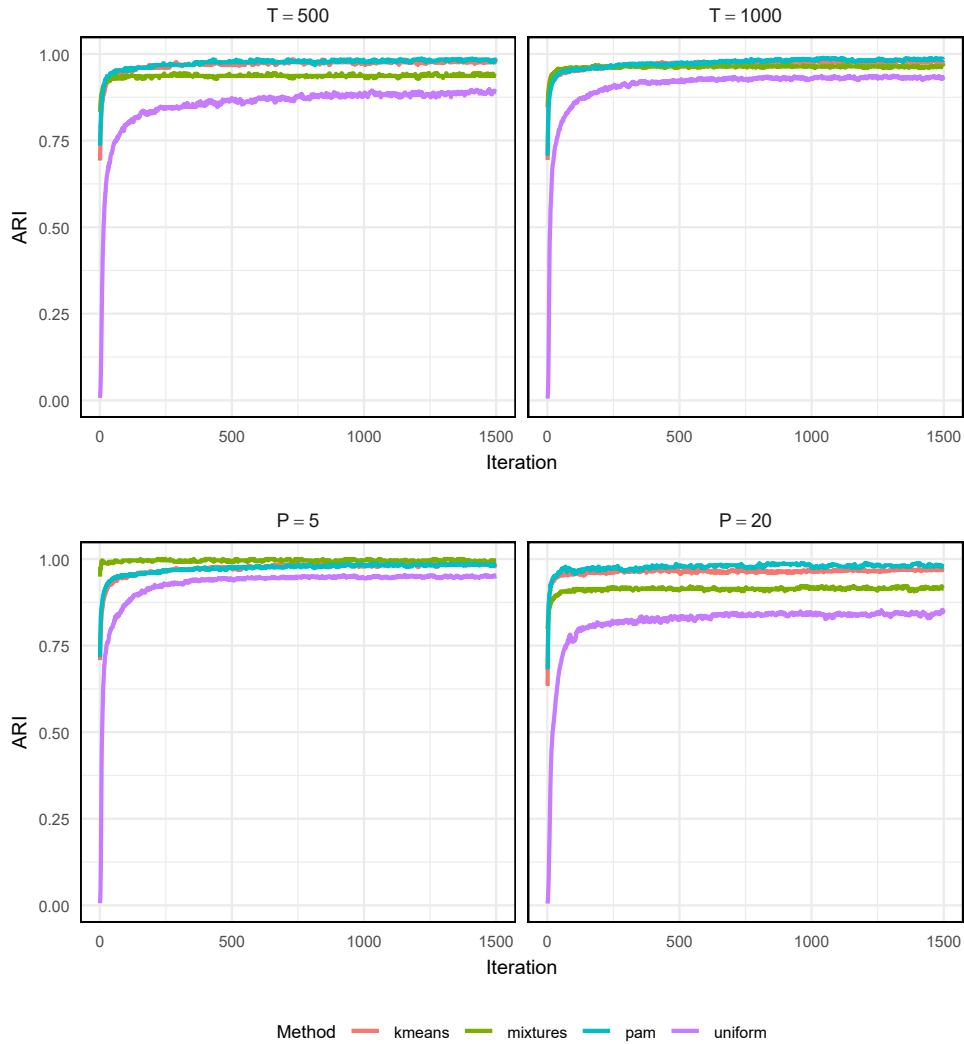


Figure 4: Median ARI across 50 seeds at each iteration, computed between true and estimated latent sequences for all initialization methods for varying  $T$  (top panel) and  $P$  (bottom). Results refer to data simulated from a Gaussian distribution.

In general, we observe that  $k$ -means achieves higher median ARI values, lower ARI variability, and narrower 95% confidence intervals across all scenarios, including the most challenging ones, such as  $\omega = 0.1$  or high number of observed variables. On the other hand, the uniform

initialization, while simple and widely used as a default method, consistently yields slowest convergence and highest variability across replications.

## 4.2 Second scenario: Student- $t$ data

The second simulation scenario employs data generated from a Student- $t$  HMM with  $\nu = 5$  degrees of freedom. This design introduced heavy-tailed behavior and within-state variability representing a realistic dataset of model misspecification, which usually arises in macroeconomic application. Figure 5 illustrates the evolution of the median ARI across iterations (top panel) and the histogram of ARI values at convergence (bottom panel) for different initialization strategies. The  $k$ -means and pam initializations converge rapidly and consistently to the correct clustering, demonstrating strong performance with median ARI above 0.9. In contrast, the mixtures and uniform initializations often fail to recover the true partition as shown by low median ARI values. This results are also highlighted by the distribution of estimated ARIs in the bottom panel, where the ARI histograms exhibit large dispersion with values in the left tail of the distribution.

Table 2 reports results for different overlap values ( $\omega = \{0, 0.1\}$ ) and true regime configurations ( $K = \{2, 4\}$ ). When the clusters are clearly separated (top-left panel),  $k$ -means and pam achieve nearly perfect classification, while mixture initialization shows a drop in the median ARI (0.86), as expected, due to its strong connection with the normality assumption. As for the Gaussian scenario, the uniform initialization has lowest median ARI and highest variability.

When increasing the value of  $\omega$ , all methods experience reduced performance due to heavier tails, but the magnitude differs substantially. The  $k$ -means and pam initializations achieve median ARI values close to 0.8, whereas the remaining methods deteriorate substantially, with the mixture initialization performing the worst (median ARI equal to 0.29).

Table 2: Median, 2.5% and 97.5% quantiles and standard deviation (SD) of ARI, and estimated number of states  $\hat{K}$ , across initialization methods, for different  $\omega$  and  $K$ , with data simulated from a Student- $t$  distribution. Highest ARI median and lowest ARI standard deviation are highlighted in bold.

Method	Median	2.5%	97.5%	SD	Median	2.5%	97.5%	SD	$\hat{K}$
$\omega = 0$					$K = 2$				
$k$ -means	<b>1.00</b>	0.73	1.00	<b>0.07</b>	<b>0.95</b>	0.57	1.00	<b>0.16</b>	<b>2</b>
mixtures	0.86	0.56	1.00	0.13	0.72	0.00	0.96	0.34	3
pam	<b>1.00</b>	0.73	1.00	<b>0.07</b>	<b>0.95</b>	0.00	1.00	0.22	<b>2</b>
uniform	0.69	0.00	1.00	0.29	0.67	0.00	1.00	0.36	4
$\omega = 0.10$					$K = 4$				
$k$ -means	<b>0.84</b>	0.00	0.97	<b>0.31</b>	0.94	0.00	1.00	<b>0.33</b>	<b>4</b>
mixtures	0.29	0.00	0.92	0.39	0.85	0.00	1.00	0.38	<b>4</b>
pam	0.82	0.00	0.97	0.36	<b>0.95</b>	0.00	1.00	0.36	<b>4</b>
uniform	0.48	0.00	0.95	0.35	0.52	0.00	1.00	<b>0.33</b>	<b>4</b>

We examine also the effect of the true number of latent states  $K$  on initialization performance. When  $K = 2$ , both mixture and uniform initializations overestimate the number of states. In contrast,  $k$ -means and pam correctly recover  $\hat{K}$  across replications. When we increase the number of states to 4, we notice that all the schemes correctly estimate the regimes, but the median ARI differs among methods, highlighting the good performance of  $k$ -means and pam with respect to mixtures and uniform.

Figure 6 shows the median ARI across iterations when varying the sequence length  $T$  (top panel) and the number of variables  $P$  (bottom panel). As  $T$  increases from 500 to 1 000,  $k$ -means and pam remain consistent and reach convergence, while mixture and uniform initializations

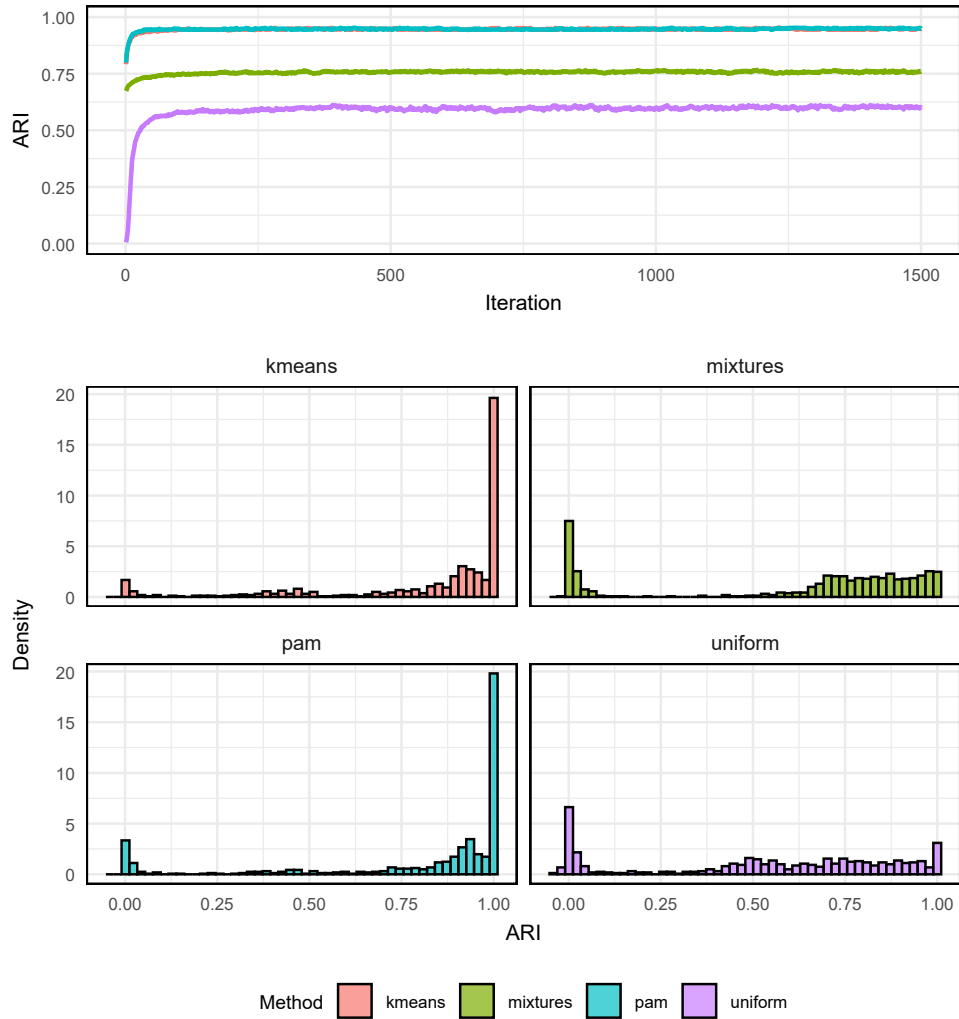


Figure 5: Median ARI across 50 seeds at each iteration computed between true and estimated latent sequences (top panel) and histograms of ARI values at convergence (bottom) for all initialization methods. Results refer to data simulated from a Student- $t$  distribution.

become less reliable with higher dimensionality. Interestingly, increasing the number of variables  $P$  (from 5 to 20) slightly favors  $k$ -means and pam in terms of accuracy.

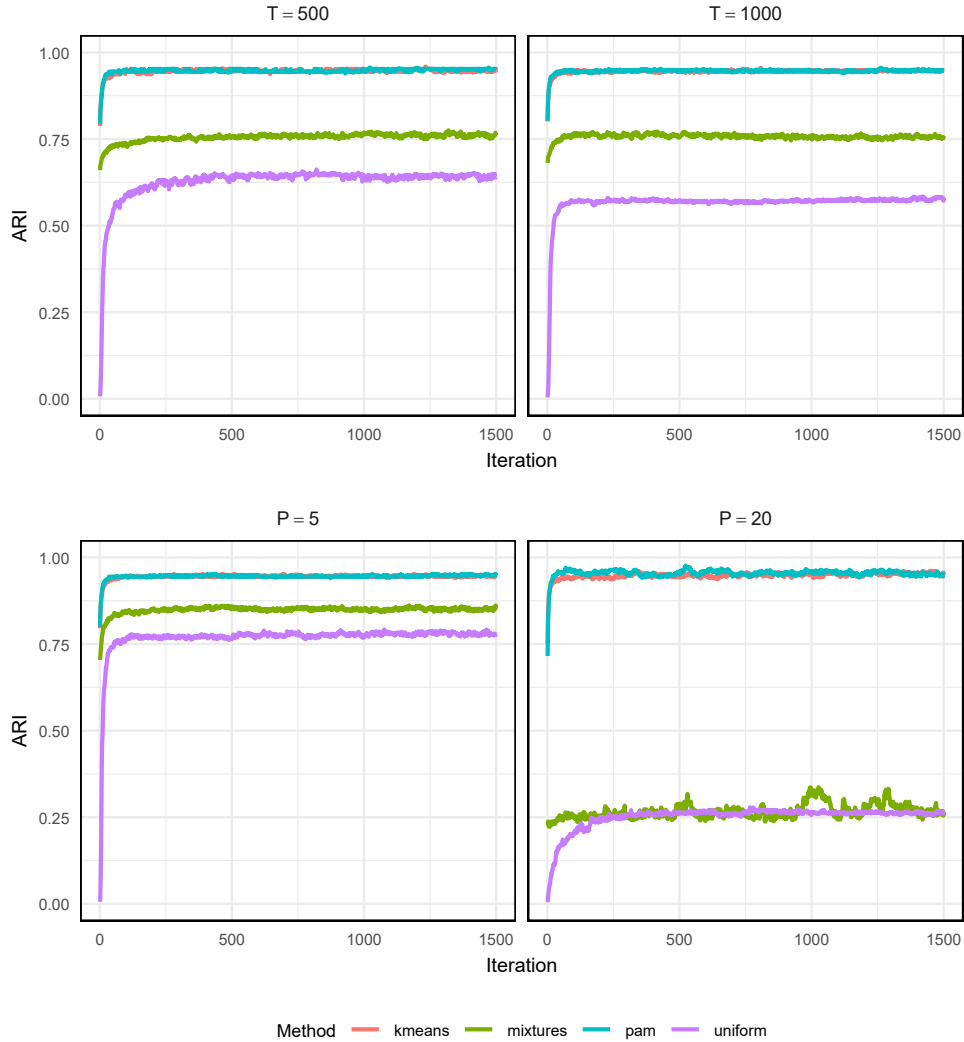


Figure 6: Median ARI across 50 seeds at each iteration, computed between true and estimated latent sequences for all initialization methods for varying  $T$  (top panel) and  $P$  (bottom). Results refer to data simulated from a Student- $t$  distribution.

To sum up, when the emission distribution deviates from a Gaussian one, uniform or mixture initializations fail to provide reliable starting partitions. As for the Gaussian scenario,  $k$ -means and pam consistently recover the highest median ARI and are similar among different overlaps, variable and time dimensionality.

### 4.3 Convergence analysis

To complement the classification evaluation of the initialization schemes, we perform different analysis of the chain convergence for the beam sampler across all the simulation settings. We assess convergence by using the classical convergence diagnostic tools and we focus on test within a chain and across different chains.

Each iHMM model is estimated for 1500 iterations, without thinning, with the first 500 discarded as burn-in. For each combination of seed,  $T$ ,  $P$ ,  $K$ , and  $\omega$ , we employ the Geweke [1992] diagnostic: for every parameter of the iHMM, we record the median success rate, defined as the share of parameters for which the absolute value of the test-statistic is lower than 2. We also compute 50% and 97.5% quantiles of autocorrelation time (ACT) across all sampled parameters, where values close to one indicating good mixing and independence of draws. Both metrics are then averaged over all runs for each initialization method and configuration.

Table 3 reports the mean and standard deviation of the Geweke success rate, together with the median and 97.5% quantile of the ACT, for different  $\omega$  and  $K$  values under Gaussian emissions. Overall, all initialization methods exhibit high Geweke success rates, indicating satisfactory convergence. The upper quantile of the ACT is considerably higher for the uniform initialization—particularly when  $\omega = 0.10$  and  $K = 2$ , while it remains below two for the other methods across all settings.

The advantage of  $k$ -means and pam can be attributed to their ability to generate structured and informative initial partitions that closely approximate the posterior mode. These initializations provide the beam sampler with a well-defined starting point, reducing the need for early-stage reallocation of latent states.

Table 3: Mean and standard deviation (SD) of the Geweke success rate, and median and 97.5% quantile of the autocorrelation time (ACT) across initialization methods, for different  $\omega$  and  $K$  values under Gaussian emissions.

Method	Geweke	SD Geweke	ACT	97.5% ACT	Geweke	SD Geweke	ACT	97.5% ACT
$\omega = 0$					$K = 2$			
$k$ -means	0.93	0.08	1.00	1.00	0.88	0.11	1.00	1.59
mixtures	0.94	0.04	1.00	1.00	0.90	0.08	1.00	1.14
pam	0.94	0.06	1.00	1.00	0.88	0.12	1.00	1.37
uniform	0.85	0.16	1.00	1.21	0.79	0.18	1.00	5.24
$\omega = 0.10$					$K = 4$			
$k$ -means	0.83	0.12	1.00	1.81	0.88	0.12	1.00	1.33
mixtures	0.84	0.11	1.00	1.32	0.88	0.11	1.00	1.31
pam	0.81	0.15	1.00	1.88	0.87	0.13	1.00	1.35
uniform	0.77	0.17	1.00	6.01	0.83	0.16	1.00	1.68

Table 4 presents the corresponding convergence diagnostics for data generated from a Student- $t$  distribution. The  $k$ -means and pam initializations maintain high Geweke success rates when  $\omega = 0$ , though these decrease as cluster overlap increases. Median ACT values remain close to one for all methods, but the 97.5% quantiles are notably higher across the board: this fact highlights the importance of running multiple chains to ensure the reliability and convergence of the results, especially when the Gaussianity assumption of the data-generating process is not guaranteed.

In conclusion,  $k$ -means and pam show higher Geweke success rate and lower ACT across both Gaussian and non-Gaussian data, while uniform initialization provides slow convergence and appears to be the most problematic scheme.

## 5 Applications

In this section, we illustrate the empirical performance of the iHMM to two real-data datasets. The first application refers to the monthly industrial production volume index, a standard macroeconomic indicator of business-cycle fluctuations, for nine European countries. This dataset is interesting in exploring regime switches since they may refer to business-cycle phases or major economic shocks. The second application analyses the different initialization schemes to the *Old Faithful* geyser dataset, a benchmark in time series clustering analysis.

Table 4: Mean and standard deviation (SD) of the Geweke success rate, and median and 97.5% quantile of the autocorrelation time (ACT) across initialization methods, for different  $\omega$  and  $K$  values under Student- $t$  emissions.

Method	Geweke	SD Geweke	ACT	97.5% ACT	Geweke	SD Geweke	ACT	97.5% ACT
$\omega = 0$					$K = 2$			
$k$ -means	0.92	0.10	1.00	1.84	0.83	0.18	1.00	2.75
mixtures	0.78	0.18	1.13	3.80	0.81	0.18	1.33	4.46
pam	0.91	0.10	1.00	2.08	0.83	0.18	1.00	3.44
uniform	0.81	0.18	1.00	3.08	0.79	0.18	1.11	4.99
$\omega = 0.10$					$K = 4$			
$k$ -means	0.73	0.20	1.11	7.03	0.82	0.18	1.00	5.76
mixtures	0.82	0.16	1.22	4.30	0.80	0.17	1.11	3.99
pam	0.74	0.21	1.12	7.60	0.83	0.19	1.00	3.31
uniform	0.78	0.17	1.12	6.57	0.80	0.17	1.00	3.49

For each dataset, we estimate the iHMM using 10 independent initialization per method ( $k$ -means, pam, Gaussian mixtures, uniform), and we set vague priors for the hyperparameters  $\alpha$  and  $\gamma$  as described in Section 3. Each chain is run for 5 000 iterations, discarding the first 3 000 as burn-in. Posterior samples from the remaining draws are used to compute parameter summaries and regime probabilities.

We first perform convergence diagnostics at the chain level, following the same procedure described in Section 4.3. We consider a chain convergent when it provides a Geweke success rate above 0.75 and a median ACT below 2. We then assess convergence across chains using the potential scale reduction factor  $\hat{R}$  [Gelman and Rubin, 1992], where values of  $\hat{R}$  close to 1 indicate good mixing and cross-chain convergence.

For the converged chains, we pool posterior draws to infer parameter estimates and regime probabilities, while obtaining temporal clustering through the *maximum a posteriori* (MAP) of these.

## 5.1 Industrial Production index data

We investigate the monthly industrial production volume index for nine European economies – Belgium, Germany, Spain, France, Italy, Lithuania, Hungary, Austria, and Romania – spanning from<sup>3</sup> March 2002 to August 2025 ( $T = 282$ ). Each series, drawn from the Eurostat database<sup>4</sup>, is seasonally and calendar adjusted, and reflects output dynamics across three main sectors: mining and quarrying; manufacturing; energy production (which includes electricity, gas, steam, and air conditioning supply).

In Figure 7, the cross-country distribution of the monthly series presents clear multimodality and heterogeneous dispersion across countries, signaling potential regime switching. Such characteristics motivate the use of iHMM, which infer both the number of unobserved macroeconomic states without restrictive parametric assumptions.

Across initialization methods, the posterior inference consistently favors  $\hat{K} = 3$ , with the exception of the uniform initialization. For the  $k$ -means initialization, all replications run yield three states, and six of them converge, with median  $\hat{R}$  values for the Gelman-Rubin test close to 1. Similarly happens for the pam initialization, where all except one run select three states and six chains converge with  $\hat{R}$  values near 1. Close to the results highlighted in the simulation section, the mixtures-based initialization also consistently identifies  $\hat{K} = 3$ , but only one chain achieves convergence, suggesting less robust sampling performance for this approach.

<sup>3</sup>In the supplementary material, we run the same analysis by excluding the COVID-19 outbreak.

<sup>4</sup>The data are available at [https://ec.europa.eu/eurostat/databrowser/view/sts\\_inpr\\_m/default/table?lang=en](https://ec.europa.eu/eurostat/databrowser/view/sts_inpr_m/default/table?lang=en)

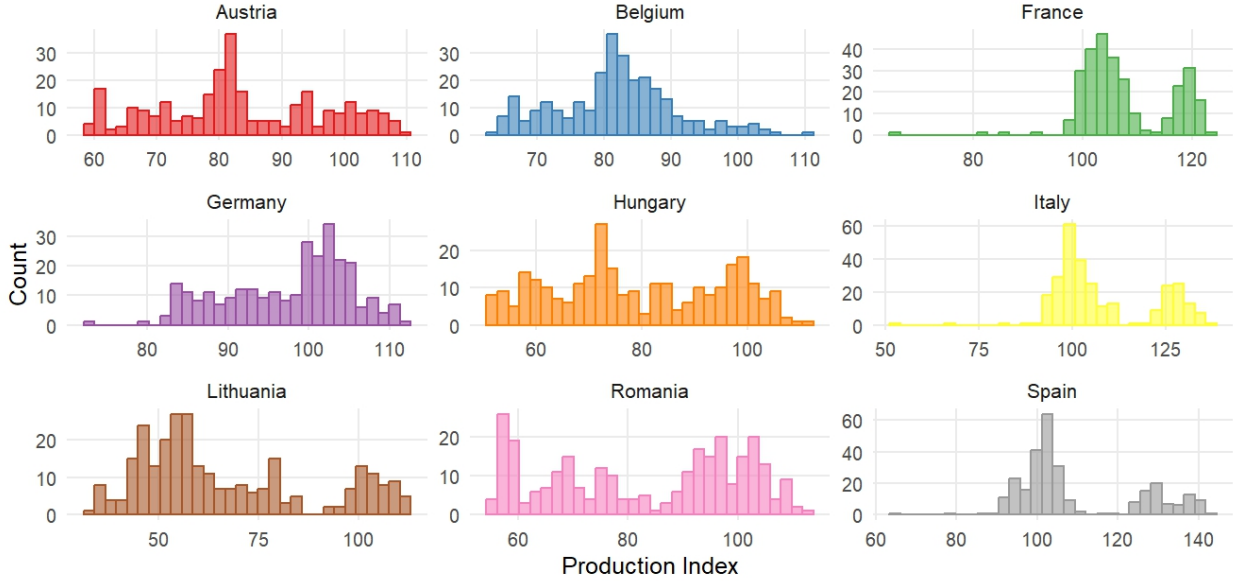


Figure 7: Empirical distributions of the industrial production index for nine European countries.

In contrast, the uniform initialization predominantly selects  $\hat{K} = 2$ , and none of these chains converge; consequently and based also on the simulation results, we omit results for this initialization method.

Table 5 reports the posterior mean of the state-conditional covariance matrices traces. The results indicate consistent regime characterization under both  $k$ -means and pam initializations, revealing three states with progressively increasing overall volatility. Similarly, Table 6 presents the state-conditional mean values for each time series. Based on the inference obtained using either the  $k$ -means or pam initialization, states 1 and 2 show broadly similar mean production index values across countries, while state 3 is characterized by higher heterogeneity, consistent with its association to the high-volatility regime.

Table 5: Trace of the covariance matrices for each inferred state and initialization method.

Method	State 1	State 2	State 3
$k$ -means	233.00	354.00	797.00
pam	215.00	377.00	792.00
mixtures	271.00	2538.00	264.00

Figure 8 illustrates the time series clustering obtained via MAP classification of the estimated regime probabilities for all initialization methods. Both  $k$ -means and pam initializations yield highly consistent classifications, as indicated by an ARI of 0.92 computed between the MAP-based state assignment sequences obtained under the two methods. They both identify four main phases in the European business cycle: an initial high-volatility, heterogeneous phase prior to the Global Financial Crisis (2002–2008), followed by a more stable one (state 2) starting in February 2012 for  $k$ -means and August 2011 for pam where the economies recovered from the crisis. Then a return to high volatility around February 2020, coinciding with the outbreak of COVID-19. This turbulent phase lasts two months for  $k$ -means and one month for pam. The subsequent period is dominated by state 1, characterized by low volatility and similar mean production index levels across countries.

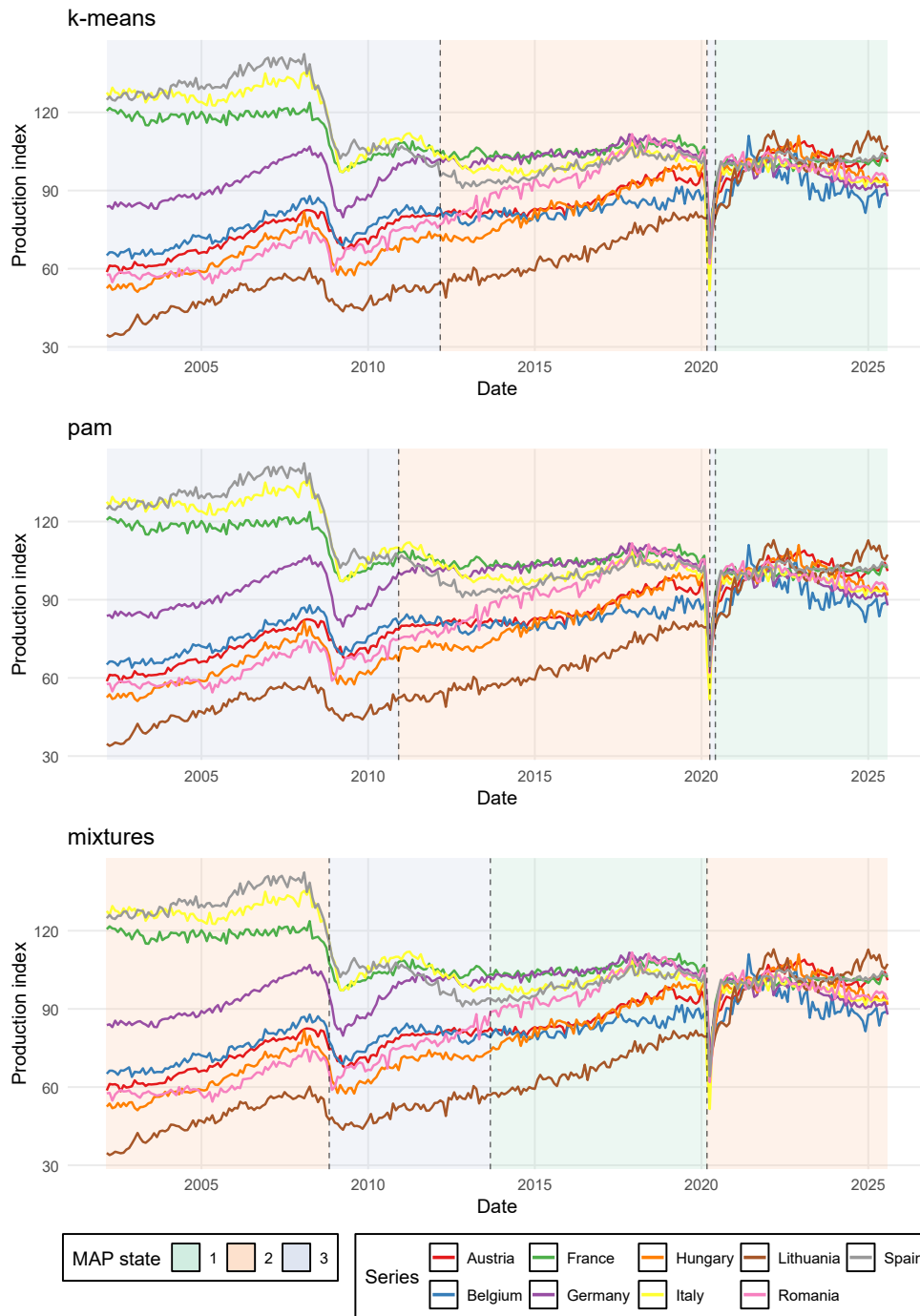


Figure 8: Regime classification over time for each initialization method, and for each country.

Table 6: State-conditional mean values by initialization method.

	Austria	Belgium	France	Germany	Hungary	Italy	Lithuania	Romania	Spain
<b><i>k</i>-means</b>									
State 1	101.25	92.65	100.39	96.22	99.74	97.03	101.34	98.48	101.19
State 2	86.54	82.82	105.27	104.42	84.29	100.77	65.96	95.27	98.74
State 3	71.60	75.16	113.11	92.48	64.34	119.93	48.72	64.99	122.41
<b>pam</b>									
State 1	101.39	92.76	100.52	96.25	99.87	97.25	101.54	98.56	101.34
State 2	86.22	82.80	105.26	104.23	83.67	100.97	65.35	94.34	98.86
State 3	71.26	74.87	113.37	92.08	64.09	120.35	48.60	64.46	123.29
<b>mixtures</b>									
State 1	87.83	83.57	105.60	105.31	87.45	100.82	68.74	98.84	99.81
State 2	83.74	82.23	109.93	94.02	79.52	113.30	71.33	78.22	117.38
State 3	77.21	78.46	103.69	95.89	67.84	104.29	51.17	74.26	101.60

Regarding the inference obtained with the Gaussian mixture initialization, Table 5 indicates a different regime structure: state 2 exhibits higher volatility, while the other two display comparable variance levels. It is not straightforward to distinguish between states 1 and 3. As shown in Table 6, the largest differences in state-conditional means occur for Lithuania, Hungary, and Romania, which exhibit substantially lower values in state 3. Four distinct phases can be identified, as illustrated in Figure 8: an initial high-volatility period ending in November 2008, a subsequent moderate-volatility phase (state 3) lasting until August 2013, a stable phase (state 1) persisting up to February 2020, and finally a high-volatility phase until the end of the observation period.

## 5.2 Old faithful geyser data

The second application analyzes the *Old Faithful* geyser data, available in the `datasets` R package. It consists of  $T = 272$  bivariate observations: the eruption duration and the waiting time to next eruption, both measured in minutes.

Across the different initialization strategies, the iHMM exhibits broadly consistent convergence behavior. Under the *k*-means initialization, seven of the ten chains estimate a median number of states equal to 2. Among these, five chains converge according to the Geweke and ACT criteria introduced earlier. Results obtained using the pam initialization are comparable: nine chains select two regimes, six of which meet the convergence criteria. When using the Gaussian mixture initialization, six chains favor three regimes, while the remaining chains estimate two states. The only two convergent chains belong to this latter group. For these three initialization methods, the Gelman–Rubin diagnostic confirms excellent mixing, with median  $\hat{R}$  values close to one across all parameters in the convergent chains. In contrast, the uniform initialization performs poorly: all chains display long ACTs, and achieve low Geweke success rates.

Figure 9 shows the classification of the observations based on the MAP state probabilities obtained under the *k*-means initialization. The results for the convergent chains using alternative initialization methods are identical. In particular, we notice two regimes that identify short eruptions followed by brief waiting times and long eruptions followed by long waiting times. These results are in line with the results obtained from prior analysis using finite HMMs and mixture models [Maruotti and Punzo, 2021].

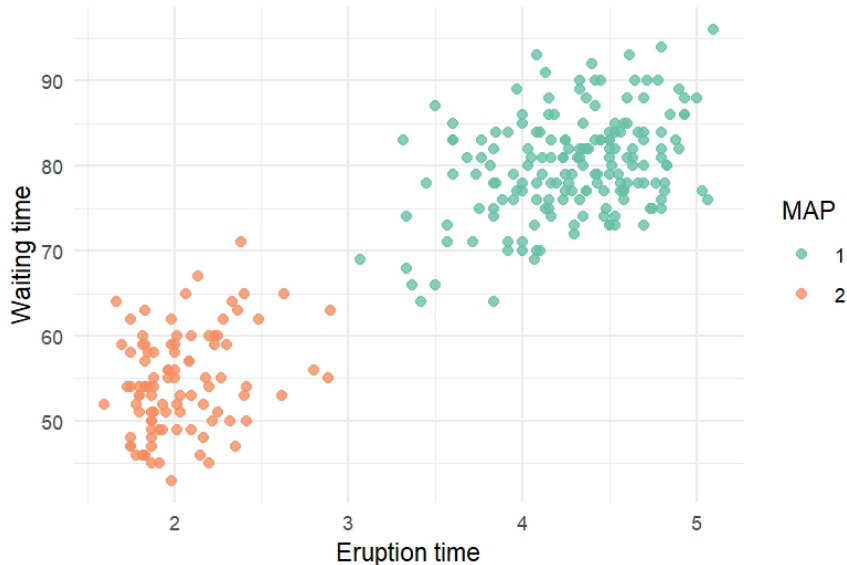


Figure 9: State classification for the *Old Faithful* geyser data based on the *maximum a posteriori* (MAP) probabilities obtained from the iHMM with  $k$ -means initialization.

## 6 Conclusions

This study highlights the impact of initialization strategies in the estimation of infinite Hidden Markov models using the beam sampling algorithm. Our results show that the choice of the initialization strategy can substantially influence the quality of the inferred latent structure and the convergence behavior of the model.

Across different simulation experiments, uniform initialization consistently underperforms, failing to recover the correct latent states even when the underlying data are generated from well-separated Gaussian mixtures. In contrast, initializations based on  $k$ -means or partitioning around medoids yield more accurate and stable estimates. While Gaussian mixture initialization remains competitive, its performance tends to deteriorate as the feature dimensionality increases or when the assumption of Gaussianity of the data is violated.

The empirical applications reinforce these findings. In the European industrial production dataset, macroeconomic phases are recovered correctly when using  $k$ -means and pam. Similarly, in the Old Faithful geyser data, the two initializations replicate the two-state dynamics. These results highlight that initialization is not a mere technical detail, but it directly affects model interpretability and computational efficiency of the infinite hidden Markov model, as is well known in the finite case.

## References

- Hirotsugu Akaike. A new look at the statistical model identification. *IEEE Transactions on Automatic Control*, 19(6):716–723, 1974.
- Francesco Bartolucci, Alessio Farcomeni, and Fulvia Pennoni. *Latent Markov models for longitudinal data*. Chapman & Hall/CRC Press, Boca Raton, FL, 2013.
- Matthew Beal, Zoubin Ghahramani, and Carl Rasmussen. The infinite hidden Markov model. *Advances in Neural Information Processing Systems*, 14:577–584, 2001.
- Christophe Biernacki, Gilles Celeux, and Gérard Govaert. Assessing a mixture model for clus-

- tering with the integrated completed likelihood. *IEEE Transactions on Pattern Analysis and Machine Intelligence*, 22(7):719–725, 2002.
- Jodie Buckby, Ting Wang, Jiancang Zhuang, and Kazushige Obara. Model checking for hidden markov models. *Journal of Computational and Graphical Statistics*, 29(4):859–874, 2020.
- Siddhartha Chib. Calculating posterior distributions and modal estimates in Markov mixture models. *Journal of Econometrics*, 75(1):79–97, 1996.
- Federico P Cortese, Fulvia Pennoni, and Francesco Bartolucci. Maximum likelihood estimation of multivariate regime switching Student-*t* copula models. *International Statistical Review*, 92(3):327–354, 2024.
- Soumita Das and Anupam Biswas. Chapter four - Analyzing correlation between quality and accuracy of graph clustering. In Ripon Patgiri, Ganesh Chandra Deka, and Anupam Biswas, editors, *Principles of Big Graph: In-depth Insight*, volume 128 of *Advances in Computers*, pages 135–163. Elsevier, 2023.
- Arthur P Dempster, Nan M Laird, and Donald B Rubin. Maximum likelihood from incomplete data via the EM algorithm. *Journal of the Royal Statistical Society: Series B*, 39(1):1–22, 1977.
- Sean R. Eddy. Profile hidden Markov models. *Bioinformatics (Oxford, England)*, 14(9):755–763, 1998.
- Christina Erlwein, Fred Espen Benth, and Rogemar Mamon. HMM filtering and parameter estimation of an electricity spot price model. *Energy Economics*, 32(5):1034–1043, 2010.
- Michael D Escobar and Mike West. Bayesian density estimation and inference using mixtures. *Journal of the American Statistical Association*, 90(430):577–588, 1995.
- Thomas S Ferguson. A Bayesian analysis of some nonparametric problems. *The Annals of Statistics*, 1(2):209–230, 1973.
- Emily B Fox, Erik B Sudderth, Michael I Jordan, and Alan S Willsky. A sticky HDP-HMM with application to speaker diarization. *The Annals of Applied Statistics*, 5(2):1020–1056, 2011.
- Chris Fraley, Adrian E. Raftery, Thomas Brendan Murphy, and Luca Scrucca. *mclust: Gaussian Mixture Modelling for Model-Based Clustering, Classification, and Density Estimation*, 2012. URL <https://cran.r-project.org/package=mclust>. R package version 4.0.
- Ruth Fuentes-García, Ramsés H Mena, and Stephen G Walker. A probability for classification based on the Dirichlet process mixture model. *Journal of Classification*, 27(3):389–403, 2010.
- Andrew Gelman and Donald B. Rubin. Inference from iterative simulation using multiple sequences. *Statistical Science*, 7(4):457–472, 1992.
- John Geweke. Evaluating the accuracy of sampling-based approaches to calculating posterior moments. In J. M. Bernardo, J. O. Berger, A. P. Dawid, and A. F. M. Smith, editors, *Bayesian Statistics 4*, pages 169–193. Clarendon Press, Oxford, UK, 1992.
- Jayanta K Ghosh and RV Ramamoorthi. *Bayesian nonparametrics*. Springer, 2003.
- Luis Gutiérrez, Eduardo Gutiérrez-Peña, and Ramsés H Mena. Bayesian nonparametric classification for spectroscopy data. *Computational Statistics & Data Analysis*, 78:56–68, 2014.
- Nils Lid Hjort, Chris Holmes, Peter Müller, and Stephen G Walker. *Bayesian nonparametrics*, volume 28. Cambridge University Press, 2010.

- Lauren Hoskovec, Matthew D Koslovsky, Kirsten Koehler, Nicholas Good, Jennifer L Peel, John Volckens, and Ander Wilson. Infinite hidden Markov models for multiple multivariate time series with missing data. *Biometrics*, 79(3):2592–2604, 2023.
- Chenghan Hou. Infinite hidden Markov switching VARs with application to macroeconomic forecast. *International Journal of Forecasting*, 33(4):1025–1043, 2017.
- Lawrence Hubert and Phipps Arabie. Comparing partitions. *Journal of Classification*, 2(1):193–218, 1985.
- Xin Jin and John M Maheu. Bayesian semiparametric modeling of realized covariance matrices. *Journal of Econometrics*, 192(1):19–39, 2016.
- Xin Jin, John M Maheu, and Qiao Yang. Bayesian parametric and semiparametric factor models for large realized covariance matrices. *Journal of Applied Econometrics*, 34(5):641–660, 2019.
- Maria Kalli, Jim E Griffin, and Stephen G Walker. Slice sampling mixture models. *Statistics and Computing*, 21(1):93–105, 2011.
- L Kaufman and PJ Rousseeuw. Clustering by means of medoids. In *Proceedings of the Statistical Data Analysis based on the  $L_1$  Norm*, pages 405–416, 1987.
- Leonard Kaufman and Peter J Rousseeuw. *Finding groups in data: An introduction to cluster analysis*. John Wiley & Sons, 2009.
- Martin Maechler, Peter Rousseeuw, Anja Struyf, Mia Hubert, and Kurt Hornik. *cluster: Cluster Analysis Basics and Extensions*, 2025. URL <https://CRAN.R-project.org/package=cluster>. R package version 2.1.8.1.
- John M Maheu and Qiao Yang. An infinite hidden Markov model for short-term interest rates. *Journal of Empirical Finance*, 38:202–220, 2016.
- Ranjan Maitra and Volodymyr Melnykov. Simulating data to study performance of finite mixture modeling and clustering algorithms. *Journal of Computational and Graphical Statistics*, 19(2):354–376, 2010.
- Antonello Maruotti and Antonio Punzo. Initialization of hidden Markov and semi-Markov models: A critical evaluation of several strategies. *International Statistical Review*, 89(3):447–480, 2021.
- Geoffrey J McLachlan and David Peel. *Finite mixture models*. John Wiley & Sons, 2000.
- Volodymyr Melnykov, Wei-Chen Chen, and Ranjan Maitra. MixSim: An R package for simulating data to study performance of clustering algorithms. *Journal of Statistical Software*, 51(12):1–25, 2012.
- Peter Müller, Fernando Andrés Quintana, Alejandro Jara, and Tim Hanson. *Bayesian nonparametric data analysis*, volume 1. Springer, 2015.
- Peter Nystrup, Henrik Madsen, and Erik Lindström. Dynamic portfolio optimization across hidden market regimes. *Quantitative Finance*, 18(1):83–95, 2018.
- Peter Nystrup, Petter N. Kolm, and Erik Lindström. Feature selection in jump models. *Expert Systems with Applications*, 184:115558, 2021.
- Silvia Pandolfi, Francesco Bartolucci, and Fulvia Pennoni. A hidden Markov model for continuous longitudinal data with missing responses and dropout. *Biometrical Journal*, 65(5):1–28, 2023.

- R Core Team. *R: A Language and Environment for Statistical Computing*. R Foundation for Statistical Computing, Vienna, Austria, 2021. URL <https://www.R-project.org/>.
- Lawrence R Rabiner. A tutorial on hidden Markov models and selected applications in speech recognition. *Proceedings of the IEEE*, 77(2):257–286, 2002.
- Gideon Schwarz. Estimating the dimension of a model. *The Annals of Statistics*, 6(2):461–464, 1978.
- Steven L Scott. Bayesian methods for hidden Markov models: Recursive computing in the 21st century. *Journal of the American Statistical Association*, 97(457):337–351, 2002.
- Jayaram Sethuraman. A constructive definition of Dirichlet priors. *Statistica Sinica*, 4(2):639–650, 1994.
- Shuping Shi and Yong Song. Identifying speculative bubbles using an infinite hidden Markov model. *Journal of Financial Econometrics*, 14(1):159–184, 2015.
- Yong Song. Modelling regime switching and structural breaks with an infinite hidden Markov model. *Journal of Applied Econometrics*, 29(5):825–842, 2014.
- Mervyn Stone. Cross-validators choice and assessment of statistical predictions. *Journal of the Royal Statistical Society: Series B (Methodological)*, 36(2):111–133, 1974.
- Yee Whye Teh, Michael I Jordan, Matthew J Beal, and David M Blei. Hierarchical Dirichlet processes. *Journal of the American Statistical Association*, 101(476):1566–1581, 2006.
- Jurgen Van Gael, Yunus Saatci, Yee Whye Teh, and Zoubin Ghahramani. Beam sampling for the infinite hidden Markov model. In *Proceedings of the 25th International Conference on Machine Learning*, pages 1088–1095, 2008.
- Oldrich Vasicek. An equilibrium characterization of the term structure. *Journal of Financial Economics*, 5(2):177–188, 1977.
- Stephen G Walker. Sampling the Dirichlet mixture model with slices. *Communications in Statistics — Simulation and Computation*, 36(1):45–54, 2007.
- Daniela M. Witten and Robert Tibshirani. A framework for feature selection in clustering. *Journal of the American Statistical Association*, 105(490):713–726, 2010.
- Qiao Yang. Stock returns and real growth: A Bayesian nonparametric approach. *Journal of Empirical Finance*, 53:53–69, 2019.
- Walter Zucchini, Iain L. MacDonald, and Roland Langrock. *Hidden Markov models for time series: An introduction using R*. CRC press, Boca Raton, FL, 2017.

## Supplementary material

Section S1 provides additional Tables and Figures from the simulation studies in Section 4 of the main paper. In Section S2, we study the macroeconomic application by excluding the COVID-19 outbreak.

### S1 Additional simulation results

#### Gaussian data

Table S1 summarizes overall performance when considering Gaussian data, showing that the  $k$ -means and pam initializations yield the highest median ARI and lowest variability.

Table S1: Median, 2.5% and 97.5% quantiles, standard deviation (SD) of ARI and median log-likelihood (LogLik) across initialization methods, for data simulated from a Gaussian distribution. Highest ARI median and lowest ARI standard deviation are highlighted in bold.

Method	Median	2.5%	97.5%	SD	LogLik
$k$ -means	<b>0.98</b>	0.38	1.00	<b>0.19</b>	-8971
mixtures	0.96	0.30	1.00	0.22	-9008
pam	0.98	0.01	1.00	0.24	-8969
uniform	0.92	0.00	1.00	0.29	-8895

Figure S1 illustrates the effect of cluster separation and the number of latent states on initialization performance for data simulated from a Gaussian distribution. The top panel reports the median ARI across iterations for different values of  $\omega$ . When  $\omega = 0$ , all methods except uniform initialization achieve perfect classification, whereas overall performance decreases when  $\omega = 0.1$ , with Gaussian mixtures converging quickly to the optimal solution. The bottom panel shows the median ARI across iterations for different true numbers of states  $K$ .  $k$ -means and pam again yield the best results, clearly outperforming Gaussian mixture initialization, particularly when  $K = 4$ .

Table S2 shows that longer sequences generally improve estimation stability, with  $k$ -means and pam consistently outperforming the others. Moreover, we observe that performance remains strong in moderate dimensions but becomes more variable as  $P$  increases. In low dimensions ( $P = 5$ ), mixture initialization achieves the most accurate result, while in higher dimensions ( $P = 20$ ), pam and  $k$ -means maintain high ARI values despite increased model complexity.

Table S3 reports the Geweke success rates and the 50 and 97.5% quantiles of the ACT across different sample lengths ( $T$ ) and dimensionalities ( $P$ ). Overall,  $k$ -means, pam, and mixtures initializations show high Geweke success rates (above 0.85) and stable convergence, while the uniform initialization performs worse, particularly for shorter series ( $T = 500$ ). The 97.5% ACT quantiles remain below 2 for most configurations, indicating efficient mixing, except for the uniform initialization.

#### Student- $t$ data

Table S4 reports the overall results when considering Student- $t$  data, showing that  $k$ -means and pam remain the most accurate and stable approaches, with the highest median ARI and lowest variability.

Figure S2 summarizes the effect of cluster separation and the number of latent states on initialization performance. The top panel shows the median ARI across iterations for different values of  $\omega$ : when  $\omega = 0$ ,  $k$ -means and pam achieve nearly perfect classification, while mixture and uniform initializations fail to reach comparable accuracy. For  $\omega = 0.1$ ,  $k$ -means and pam remain the best-performing strategies, whereas mixture initialization reaches only about 0.30

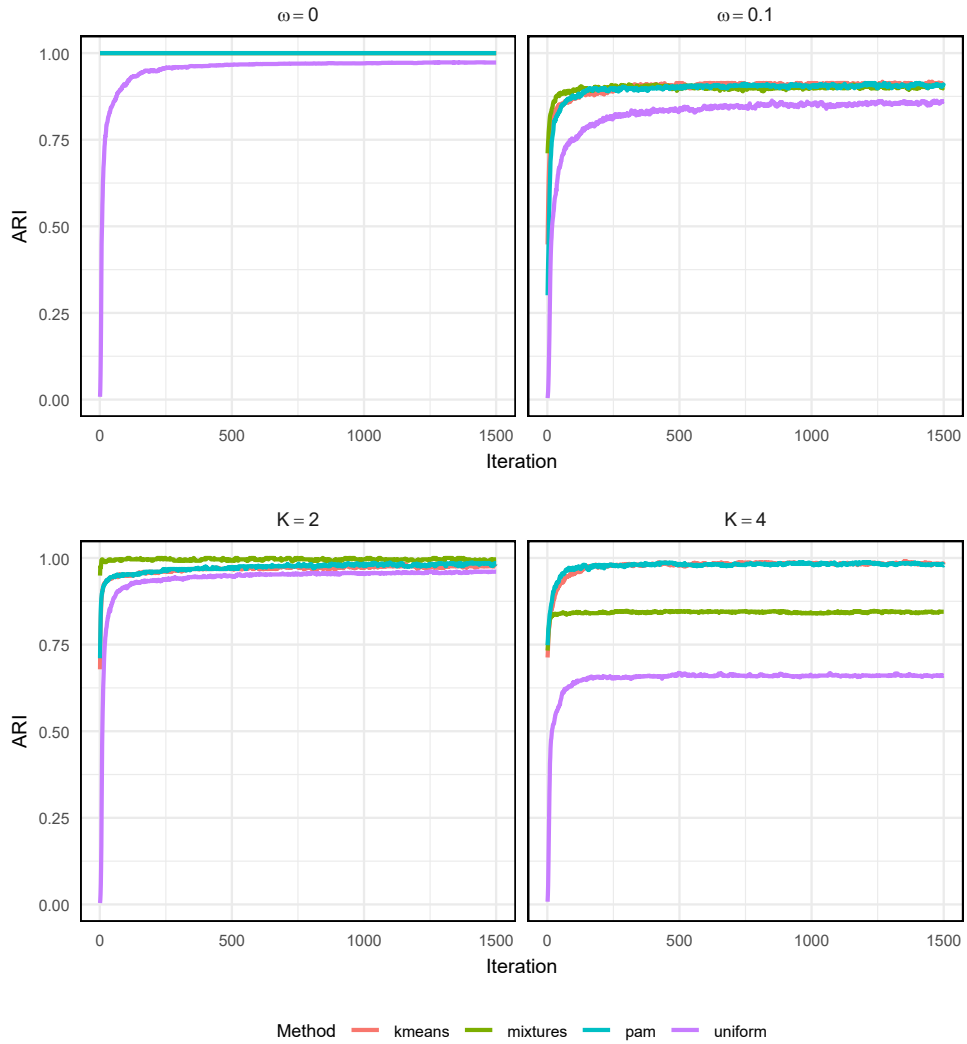


Figure S1: Top panel: median ARI across 50 seeds at each iteration, computed between true and estimated latent sequences for all initialization methods, for different  $\omega$  values. Bottom panel: median ARI across 50 seeds at each iteration for different true numbers of states  $K$ . Results refer to data simulated from a Gaussian distribution.

Table S2: Median, 2.5% and 97.5% quantiles and standard deviation (SD) of ARI across initialization methods, for different  $T$  and  $P$  values, with data simulated from a Gaussian distribution. Highest ARI median and lowest ARI standard deviation are highlighted in bold.

Method	Median	2.5%	97.5%	SD	Median	2.5%	97.5%	SD
$T = 500$								
				$P = 5$				
$k$ -means	<b>0.98</b>	0.35	1.00	<b>0.20</b>	0.99	0.46	1.00	0.13
mixtures	0.94	0.00	1.00	0.25	<b>1.00</b>	0.65	1.00	<b>0.11</b>
pam	<b>0.98</b>	0.00	1.00	0.28	0.98	0.48	1.00	0.13
uniform	0.90	0.00	1.00	0.35	0.95	0.45	1.00	0.17
$T = 1000$								
				$P = 20$				
$k$ -means	<b>0.98</b>	0.42	1.00	<b>0.18</b>	0.97	0.33	1.00	<b>0.24</b>
mixtures	0.96	0.34	1.00	0.19	0.94	0.00	1.00	0.28
pam	<b>0.98</b>	0.39	1.00	0.20	<b>0.98</b>	0.00	1.00	0.30
uniform	0.94	0.39	1.00	0.21	0.84	0.00	1.00	0.35

Table S3: Mean and standard deviation (SD) of Geweke success rate, and median and 97.5% quantile of the autocorrelation time (ACT) across initialization methods, for different  $T$  and  $P$  values.

Method	Geweke	SD Geweke	ACT	97.5% ACT	Geweke	SD Geweke	ACT	97.5% ACT
$T = 500$								
				$P = 5$				
$k$ -means	0.87	0.12	1.00	1.42	0.88	0.12	1.00	1.81
mixtures	0.88	0.12	1.00	1.32	0.90	0.09	1.00	1.23
pam	0.86	0.15	1.00	1.73	0.87	0.13	1.00	1.61
uniform	0.81	0.17	1.00	2.18	0.85	0.16	1.00	6.01
$T = 1000$								
				$P = 20$				
$k$ -means	0.88	0.11	1.00	1.56	0.88	0.11	1.00	1.20
mixtures	0.91	0.07	1.00	1.12	0.88	0.10	1.00	1.18
pam	0.88	0.11	1.00	1.23	0.87	0.13	1.00	1.24
uniform	0.81	0.17	1.00	3.58	0.77	0.16	1.00	1.20

Table S4: Median, 2.5% and 97.5% quantiles, standard deviation (SD) of ARI and median log-likelihood (LogLik) across initialization methods, for data simulated from a Student- $t$  distribution. Highest ARI median and lowest ARI standard deviation are highlighted in bold.

Method	Median	2.5%	97.5%	SD	LogLik
$k$ -means	<b>0.95</b>	0.01	1.00	<b>0.27</b>	-8756
mixtures	0.76	0.00	1.00	0.36	-8941
pam	<b>0.95</b>	0.00	1.00	0.31	-8748
uniform	0.59	0.00	1.00	0.34	-9393

in ARI. The bottom panel reports the median ARI across iterations for different true numbers of states  $K$ . pam and  $k$ -means again deliver the best results, outperforming Gaussian mixture initialization in both accuracy and convergence speed.

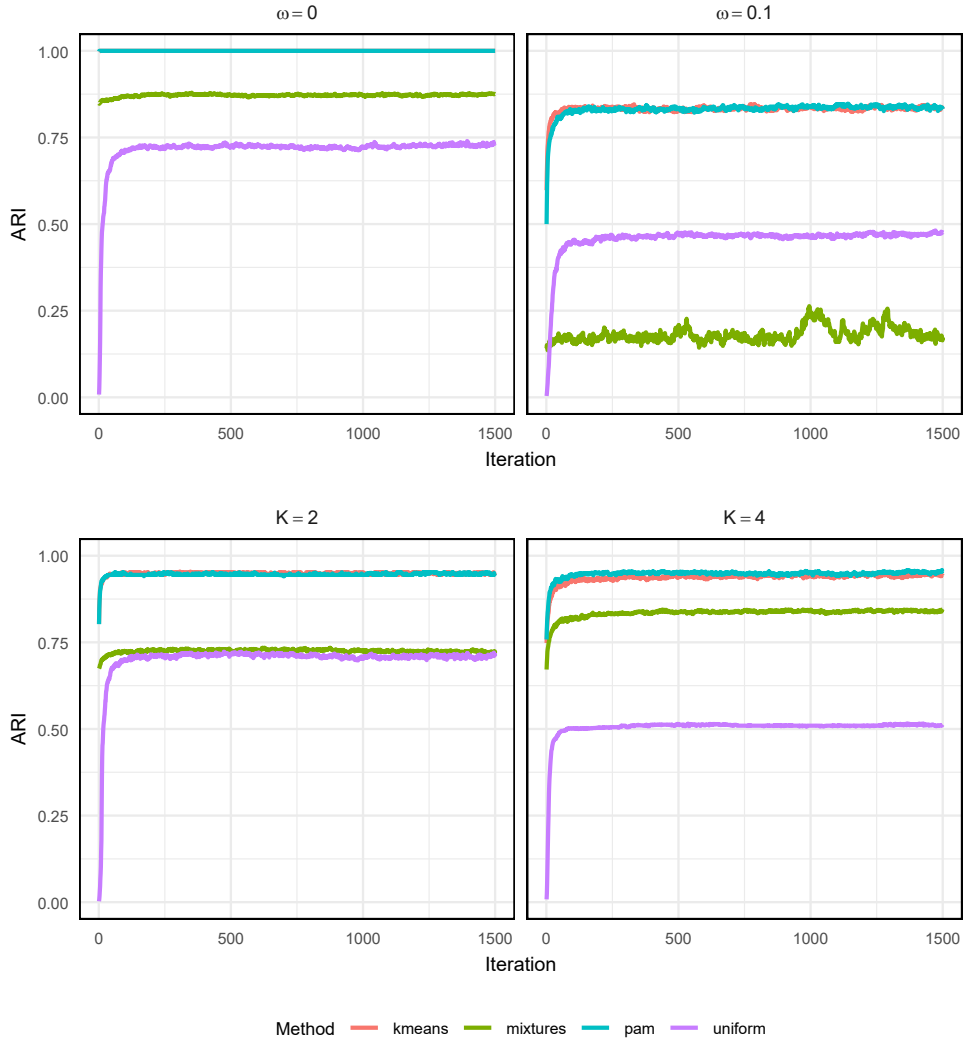


Figure S2: Top panel: median ARI across 50 seeds at each iteration, computed between true and estimated latent sequences for all initialization methods, for different  $\omega$  values. Bottom panel: median ARI across 50 seeds at each iteration for different true numbers of states  $K$ . Results refer to data simulated from a Student- $t$  distribution.

Table S5 summarizes results for varying sequence length  $T$  and number of variables  $P$ . Increasing  $T$  has small effect on performance, while higher dimensionality ( $P = 20$ ) leads to slightly lower accuracy and greater variability across initialization methods, particularly for mixtures and uniform initialization.

Table S6 summarizes the Geweke success rates and the 50 and 97.5% ACT quantiles for different time lengths ( $T$ ) and dimensionalities ( $P$ ) under Student- $t$  emissions. Overall, Geweke success rates are slightly lower than in the Gaussian case. Nevertheless,  $k$ -means and pam maintain relatively stable convergence, while mixtures and uniform initializations show more variability, particularly for shorter series and smaller  $P$ . The 97.5 % ACT quantiles are generally higher

Table S5: Median, 2.5% and 97.5% quantiles and standard deviation (SD) of ARI across initialization methods, for different  $T$  and  $P$  values, with data simulated from a Student- $t$  distribution. Highest ARI median and lowest ARI standard deviation are highlighted in bold.

Method	Median	2.5%	97.5%	SD	Median	2.5%	97.5%	SD
$T = 500$								
$k$ -means	<b>0.97</b>	0.01	1.00	<b>0.28</b>	<b>0.95</b>	0.44	1.00	0.16
mixtures	0.76	0.00	1.00	0.37	0.84	0.61	1.00	<b>0.12</b>
pam	0.96	0.00	1.00	0.31	<b>0.95</b>	0.46	1.00	0.15
uniform	0.62	0.00	1.00	0.37	0.76	0.38	1.00	0.20
$T = 1000$								
$k$ -means	<b>0.94</b>	0.01	1.00	<b>0.26</b>	0.97	0.00	1.00	<b>0.34</b>
mixtures	0.76	0.00	0.99	0.36	0.20	0.00	0.92	0.39
pam	<b>0.94</b>	0.00	1.00	0.30	<b>0.98</b>	0.00	1.00	0.39
uniform	0.56	0.00	1.00	0.32	0.26	0.00	0.91	0.32

across all methods.

Table S6: Mean and standard deviation (SD) of Geweke success rate, and median and 97.5% quantile of the autocorrelation time (ACT) across initialization methods, for different  $T$  and  $P$  values (Student- $t$  data).

Method	Geweke	SD Geweke	ACT	97.5% ACT	Geweke	SD Geweke	ACT	97.5% ACT
$T = 500$								
$k$ -means	0.83	0.18	1.00	3.91	0.82	0.17	1.00	2.93
mixtures	0.80	0.18	1.15	4.84	0.77	0.17	1.46	5.21
pam	0.82	0.20	1.00	3.98	0.81	0.17	1.00	3.32
uniform	0.79	0.17	1.00	4.53	0.77	0.19	1.26	6.75
$T = 1000$								
$k$ -means	0.82	0.18	1.00	2.67	0.83	0.20	1.00	6.34
mixtures	0.80	0.16	1.20	3.72	0.84	0.17	1.12	2.15
pam	0.84	0.17	1.00	3.26	0.84	0.20	1.00	5.22
uniform	0.80	0.18	1.05	4.64	0.82	0.16	1.00	2.18

## S2 Empirical analysis on industrial production index data excluding the COVID-19 period

We replicate the analysis of Section 5.1 using data up to January 2020, just before the COVID-19 outbreak. Across initialization methods, the iHMMs consistently identify two latent states ( $K = 2$ ), corresponding to low- and high-volatility regimes. The estimated covariance traces in Table S7 confirm this pattern, with the high-volatility state exhibiting roughly twice the overall variability of the low-volatility one. State-conditional mean levels, reported in Table S8, are also highly consistent across initialization methods. Figure S3 shows the temporal regime classification based on the maximum a posteriori of estimated state probabilities. Change points are detected on February 2012 for the  $k$ -means and pam initializations, and on September 2011 for the mixtures initialization.

Table S7: Trace of the covariance matrices for each inferred state and initialization method.

Method	State 1	State 2
$k$ -means	337.00	652.00
pam	340.00	647.00
mixtures	357.00	622.00

Table S8: State-conditional mean values by initialization method.

	Austria	Belgium	France	Germany	Hungary	Italy	Lithuania	Romania	Spain
<b><math>k</math>-means</b>									
State 1	86.63	82.79	105.24	104.50	84.45	100.62	66.18	95.63	98.63
State 2	71.74	75.28	113.68	92.98	64.38	120.65	48.33	65.16	122.87
<b>pam</b>									
State 1	86.53	82.78	105.24	104.46	84.32	100.68	66.00	95.44	98.65
State 2	71.59	75.19	113.78	92.84	64.25	120.87	48.24	64.97	123.15
<b>mixtures</b>									
State 1	86.28	82.73	105.26	104.34	83.83	100.87	65.45	94.65	98.68
State 2	71.32	74.99	114.03	92.56	64.01	121.35	48.12	64.63	123.92

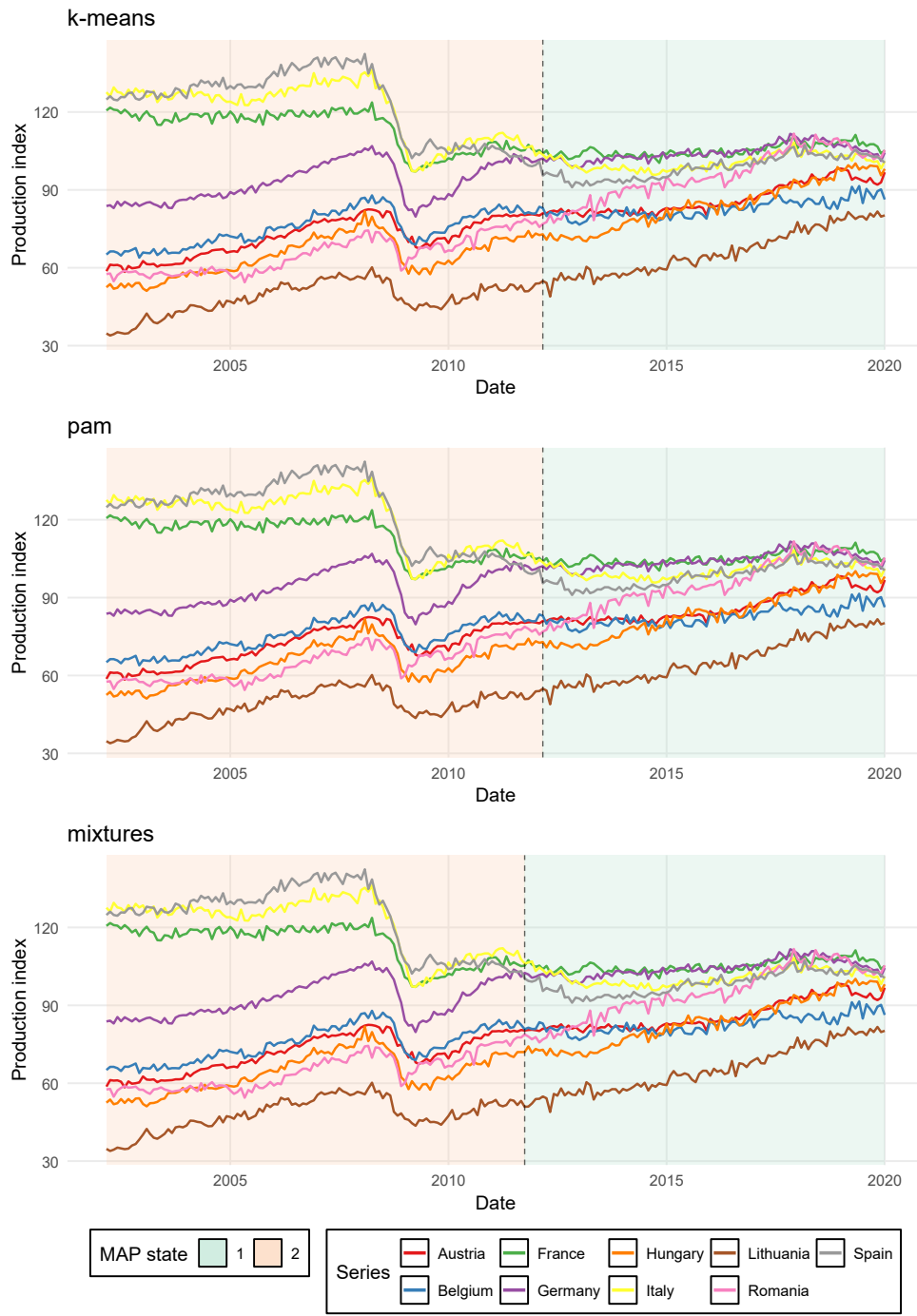


Figure S3: Regime classification over time for each initialization method, and production index time series of each country.